CEST-2.2 overexpression alters lipid metabolism and extends longevity of mitochondrial mutants

Antonia Piazzesi[1,†] (iD), Yiru Wang[1,†] (iD), Joshua Jackson[1,†] (iD), Lena Wischhof[1] (iD), Viktoria Zeisler-Diehl[2], Enzo Scifo[1] (iD), Ina Oganezova[1] (iD), Thorben Hoffmann[1] (iD), Pablo Gómez Martín[1], Fabio Bertan[1], Chester J J Wrobel[3], Frank C Schroeder[3], Dan Ehninger[1], Kristian Händler[1,4], Joachim L Schultze[1,4,5], Lukas Schreiber[2] (iD), Gerhild van Echten-Deckert[6] (iD), Pierluigi Nicotera[1] (iD) & Daniele Bano[1,*] (iD)

Abstract

Mitochondrial dysfunction can either extend or decrease *Caenorhabditis elegans* lifespan, depending on whether transcriptionally regulated responses can elicit durable stress adaptation to otherwise detrimental lesions. Here, we test the hypothesis that enhanced metabolic flexibility is sufficient to circumvent bioenergetic abnormalities associated with the phenotypic threshold effect, thereby transforming short-lived mitochondrial mutants into long-lived ones. We find that CEST-2.2, a carboxylesterase mainly localizes in the intestine, may stimulate the survival of mitochondrial deficient animals. We report that genetic manipulation of *cest-2.2* expression has a minor lifespan impact on wild-type nematodes, whereas its overexpression markedly extends the lifespan of complex I-deficient *gas-1(fc21)* mutants. We profile the transcriptome and lipidome of *cest-2.2* overexpressing animals and show that CEST-2.2 stimulates lipid metabolism and fatty acid beta-oxidation, thereby enhancing mitochondrial respiratory capacity through complex II and LET-721/ETFDH, despite the inherited genetic lesion of complex I. Together, our findings unveil a metabolic pathway that, through the tissue-specific mobilization of lipid deposits, may influence the longevity of mitochondrial mutant *C. elegans*.

Introduction

Mitochondria contribute to energy production and host biosynthetic reactions that supply molecules for metabolic and signaling processes. Through iterative oxidation of nutrients (e.g., sugars, amino acids, and fatty acids), mitochondria generate reducing equivalents in the form of metabolic intermediates, NADH, and $FADH_2$ (Spinelli & Haigis, 2018; Martinez-Reyes & Chandel, 2020). The exothermic transfer of electrons from these reduced molecules to the electron transport chain (ETC) and then to oxygen is used by the respiratory complexes (i.e., complex I, complex III, and complex IV) to drive protons from the matrix to the intermembrane space. The subsequent dissipation of the electrochemical gradient across the inner membrane promotes ATP biosynthesis and thermogenesis, ROS production, and ion transport (Martinez-Reyes & Chandel, 2020; Sies & Jones, 2020). All these processes influence cell division, differentiation, maintenance, and demise, thereby contributing to animal development, growth, and survival.

A large literature has described an increasing number of genetic lesions and environmental toxins that alter mitochondrial oxidative phosphorylation (OXPHOS) and can elicit human metabolic disorders and neurodegenerative conditions, further emphasizing the relevance of mitochondria in human pathophysiology (Schon & Przedborski, 2011; Koopman *et al*, 2012; Gorman *et al*, 2016; Bano & Prehn, 2018; Wallace, 2018; Frazier *et al*, 2019). Despite the profound clinical importance, currently available therapeutic interventions are mostly symptomatic, since they may improve the life quality of the patients without substantially modifying the progression of the disease (Gorman *et al*, 2016; Russell *et al*, 2020). Other challenges include a better understanding of the molecular mechanisms that can counteract mitochondrial dysfunction, which may help to single out novel targets potentially relevant for therapeutic purposes. In this regard, preclinical studies in recent years have

1 German Center for Neurodegenerative Diseases (DZNE), Bonn, Germany
2 Institute of Cellular and Molecular Botany (IZMB), University of Bonn, Bonn, Germany
3 Boyce Thompson Institute and Department of Chemistry and Chemical Biology, Cornell University, Ithaca, NY, USA
4 PRECISE Platform for Single Cell Genomics and Epigenomics, German Center for Neurodegenerative Diseases (DZNE), University of Bonn, Bonn, Germany
5 Department for Genomics and Immunoregulation, LIMES Institute, University of Bonn, Bonn, Germany
6 LIMES Institute for Membrane Biology and Lipid Biochemistry, University of Bonn, Bonn, Germany
*Corresponding author. Tel: +49 228 43302 510; Fax: +49 228 43302 689; E-mail: daniele.bano@dzne.de
†These authors contributed equally to this work

described innovative genetic and pharmacological approaches that improve organismal fitness by stimulating transcriptional programs that buffer toxic species and enhance the usage of available resources. Consistent with this concept, it was shown that inhibition of mTOR signaling ameliorates aberrant processes linked to mitochondrial dysfunction by shifting metabolism toward catabolism (Johnson *et al*, 2013; Ising *et al*, 2015; Peng *et al*, 2015; Zheng *et al*, 2016; Khan *et al*, 2017; Siegmund *et al*, 2017; Wischhof *et al*, 2018; Gioran *et al*, 2019). Similarly, chronic exposure to moderate hypoxia alleviates metabolic defects and triggers adaptive pathways that limit the damage due to impaired mitochondrial bioenergetics, thereby stimulating the survival of animals carrying mitochondrial genetic lesions (Jain *et al*, 2016, 2019, 2020; Ast *et al*, 2019; To *et al*, 2019; Grange *et al*, 2021). As additional examples, supplementation of nicotinamide mononucleotide, and pharmacological and genetic manipulations of the redox state improve the metabolic derangement due to NAD$^+$ depletion in mitochondrial deficient cells (Canto *et al*, 2012; Karamanlidis *et al*, 2013; Mouchiroud *et al*, 2013; Cerutti *et al*, 2014; Pirinen *et al*, 2014; Cracan *et al*, 2017; Liu *et al*, 2021). Based on these converging lines of evidence, eukaryotic cells are capable of responding to defective mitochondrial energy production by establishing transcriptional activities and broad metabolic reprogramming that channel resources to build up protective mechanisms against long-lasting systemic changes. In the context of human pathophysiology, it is crucial to decode this stress response network, since it may provide molecular targets that are therapeutically valuable for chronic and/or inherited diseases associated with mitochondrial lesions (Lardenoije *et al*, 2015; Riera *et al*, 2016; Mottis *et al*, 2019).

The mitochondrial threshold effect theory assumes that phenotypic presentations of mitochondrial dysfunction occur when a critical state is reached and functional compensation is irremediably compromised (Rossignol *et al*, 2003), however, it remains elusive, which are the key metabolic processes that dictate the trade-off between growth, reproduction, and somatic maintenance during adverse conditions. The nematode *Caenorhabditis elegans* has proven to be a useful *in vivo* model organism to investigate the mitochondrial threshold effect in stress resilience and lifespan-extending programs (Riera *et al*, 2016; Shpilka & Haynes, 2018). During *C. elegans* development (Feng *et al*, 2001; Dillin *et al*, 2002; Rea *et al*, 2007), mild disruption of the mitochondrial ETC activity impairs OXPHOS and evokes a profound transcriptional reprogramming that alleviates the chronic energy crisis. Along with a considerable shift toward catabolic processes (Gioran *et al*, 2019), transcriptional activation of unfolded protein response (UPR) and expression of detoxifying enzymes (e.g., SOD-3 and GST-4) prevent the detrimental collapse of cellular proteostasis (Lin & Haynes, 2016; Tian *et al*, 2016b; Shpilka & Haynes, 2018). In a cell-nonautonomous fashion, secretion of signals (e.g., ROS, neurotransmitters, and hormones) from mitochondrial deficient cells can communicate adverse conditions throughout the whole organism. In this regard, the enhanced responsiveness to stressful states presumably elicits global protective mechanisms that have beneficial effects on animal survival (Durieux *et al*, 2011). These broad physiological changes require a permissive chromatin landscape for the engagement and establishment of transcriptional programs that control homeostatic processes (Benedetti *et al*, 2006; Haynes *et al*, 2010; Nargund *et al*, 2012; Merkwirth *et al*, 2016; Piazzesi *et al*, 2016;

Tian *et al*, 2016a). In this regard, we previously reported that aberrant chromatin remodeling due to the loss of replication-independent histone H3.3 (i.e., the main H3 variant that is expressed in postmitotic cells and accumulates during aging) impairs the establishment of lifespan-extending programs, including those dependent on mitochondria (Troulinaki & Bano, 2012; Piazzesi *et al*, 2016; Bano *et al*, 2017). Consistently, altered histone H3 methylation compromises the transcriptional activation of mitochondrial unfolded protein response (UPR^{mt}) and, consequently, shortens the lifespan of mitochondrial *C. elegans* mutants (Merkwirth *et al*, 2016; Tian *et al*, 2016a, 2016b). Thus, these lines of evidence suggest that epigenetic plasticity can confer physiological fitness to multicellular organisms. If so, this concept raises a very basic question: can we transform sick, short-lived mitochondrial mutants into long-lived ones?

Here, we report that overexpression of a single enzyme is sufficient to potentiate the residual respiratory capacity of complex I-deficient nematodes by redirecting lipid usage toward fatty acid beta-oxidation. Through multiomics analyses coupled with conventional epistatic studies, we demonstrate a previously unknown metabolic network that can extend *C. elegans* lifespan, with molecular aspects that may be partially conserved in some disease settings in higher metazoa. More broadly, our findings emphasize the strength of adaptive mechanisms in promoting epigenetic reprogramming that sustains survival of animals carrying mitochondrial lesions.

Results

CEST-2.2 expression influences the lifespan of complex I mutant nematodes

We previously reported that H3.3 expression establishes lifespan-extending programs in *C. elegans* by supporting transcriptional plasticity underlying stress resilience (Piazzesi *et al*, 2016). Based on that, we hypothesized that H3.3 may be differently loaded onto chromatin in long-lived mitochondrial mutants compared with short-lived ones. To test this hypothesis, we employed animals carrying either *nuo-6(qm200)* or *gas-1(fc21)* alleles, both altering complex I activity, but extending or reducing *C. elegans* lifespan, respectively (Fig EV1A and Appendix Table S1). Using wild-type (wt) and mitochondrial mutant animals expressing GFP-tagged HIS-72 (Ooi *et al*, 2006; Piazzesi *et al*, 2016), we performed chromatin immunoprecipitation (ChIP) followed by deep sequencing (Fig 1A), focusing our analysis exclusively on promoter regions. We found that HIS-72::GFP was loaded onto the promoters of 996 genes and 917 genes in *nuo-6(qm200)* and *gas-1(fc21)* mutant nematodes, respectively (Fig 1B). Of these, 711 genes overlapped between the two strains, with 591 of those also being shared with wt nematodes (Fig 1B). We investigated the expression profiles of the 179 genes in which H3.3-enriched promoters were exclusively detected in the long-lived *nuo-6(qm200)* mutants. We employed the respective RNA-seq datasets from these mutants (Piazzesi *et al*, 2016; Gioran *et al*, 2019) and found that 10 of these genes were consistently downregulated in *gas-1(fc21)* mutants, upregulated in *nuo-6 (qm200)* mutants but downregulated in *nuo-6(qm200)*, *his-72 (tm2066)*, *and his-71(ok2289)* triple mutant animals, consistent with their transcription being modulated by the presence of H3.3 (Fig 1C and D). Of these 10 genes, 5 of them encode evolutionarily
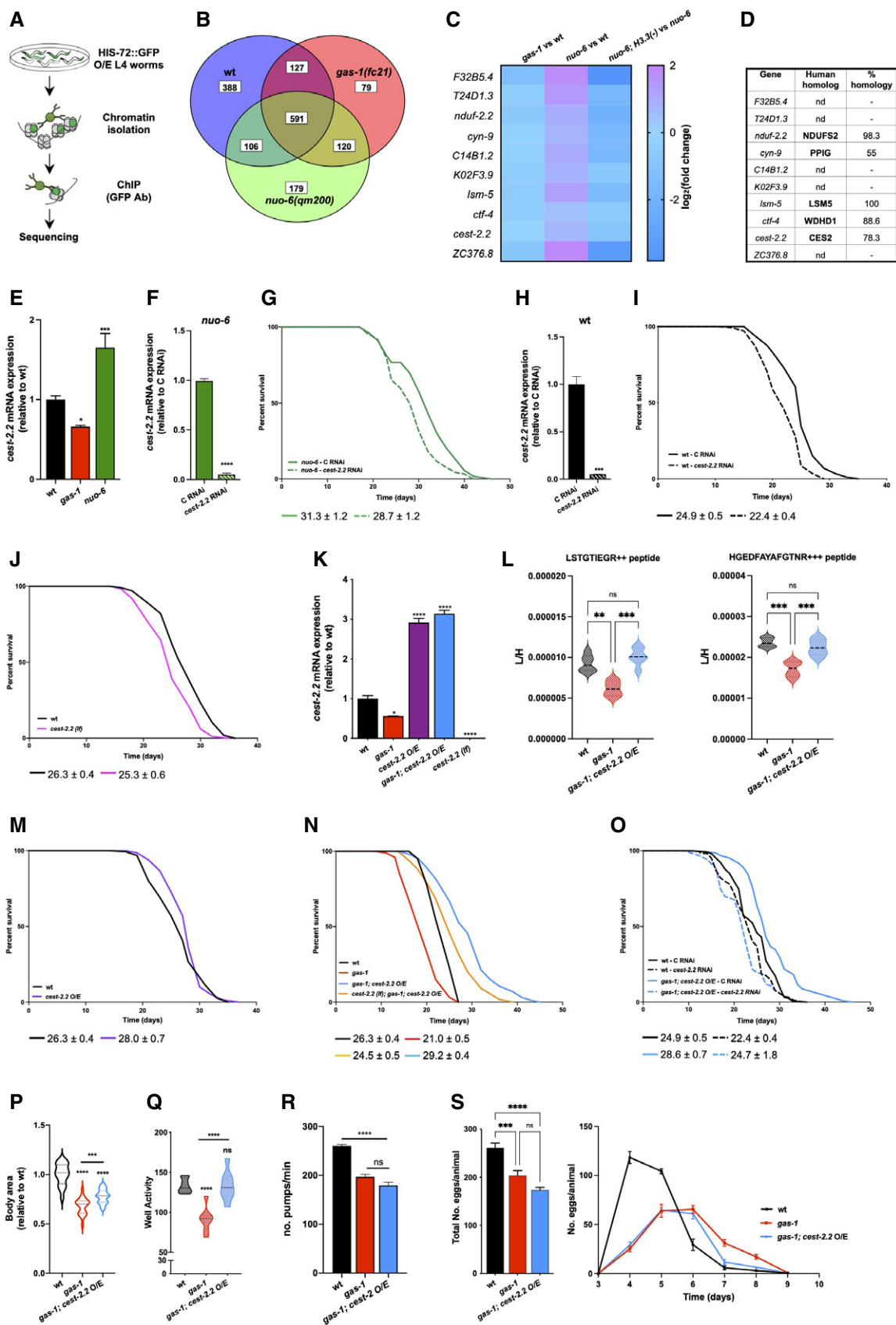
Figure 1.

Figure 1. CEST-2.2 expression influences the lifespan of mitochondrial mutant *C. elegans*.

A   Schematic representation of ChIP-Seq strategy. An antibody against GFP was used to immunoprecipitate HIS-72::GFP loaded onto chromatin. Subsequent DNA sequencing was performed onto immunoprecipitated chromatin.
B   Venn diagram of genes with H3.3-enriched promoters between wt (blue), *gas-1(fc21)* (red), and *nuo-6(qm200)* (green) mutants.
C   Heatmap of genes with H3.3-enriched promoters exclusively in *nuo-6(qm200)* mutants, downregulated in *gas-1(fc21)* versus wt, upregulated in *nuo-6(qm200)* versus wt, and downregulated in *nuo-6(qm200); his-72(tm2066); his-71(ok2289)* versus *nuo-6(qm200)*.
D   Table of genes with H3.3-enriched promoters exclusively in *nuo-6(qm200)* nematodes, whose gene expression was upregulated in *nuo-6(qm200)* versus wt, downregulated in *gas-1(fc21)* versus wt, and downregulated in *nuo-6(qm200); his-72(tm2066); his-71(ok2289)* versus *nuo-6(qm200)*. Human orthologs and corresponding % homology are indicated.
E   qRT-PCR of *cest-2.2* in wt, *gas-1(fc21)*, and *nuo-6(qm200)* mutants (one-way ANOVA with Dunnet's *post-hoc* correction, *n* = 9–12 technical replicates pooled from three independent experiments).
F   qRT-PCR of *cest-2.2* mRNA expression in *nuo-6(qm200)* animals grown on control and *cest-2.2* RNAi (unpaired *t*-test, *n* = 3 biological replicates).
G   Representative survival curves of *nuo-6(qm200)* mutants fed with control (C RNAi) and dsRNA against *cest-2.2*.
H   qRT-PCR of *cest-2.2* mRNA expression in wt animals grown on control and *cest-2.2* RNAi (unpaired *t*-test, *n* = 3 biological replicates).
I   Lifespan assay of wt animals grown on control and *cest-2.2* RNAi.
J   Representative survival curves of wt and *cest-2.2 (lf)* nematodes.
K   qRT-PCR of *cest-2.2* mRNA expression in wt, *gas-1(fc21)*, *gas-1(fc21); cest-2.2 O/E* and *cest-2.2 (lf)* nematodes (one-way ANOVA with Dunnett's *post-hoc* correction, *n* = 3 biological replicates).
L   SureQuant-based quantitative mass spectrometry analysis of CEST-2.2 protein levels. Light/heavy ratios (L/H) of the two unique CEST-2.2 peptides (LSTGTIEGR and HGEDFAYAFGTNR) used for quantitation are represented as violin plots (*n* = 3 for wt and *gas-1; cest-2.2 O/E*, *n* = 2 for *gas-1*; the *n* of analyzed samples per group refers to biological replicates of pooled nematodes from a single plate; the median is indicated with a dashed line). Statistical analysis was performed using the nonparametric *t*-test.
M   Representative survival curves of wt and *cest-2.2(lf)* nematodes.
N   Lifespan assay of wt, *gas-1(fc21)*, *gas-1(fc21); cest-2.2 O/E* and *cest-2.2(lf); gas-1(fc21); cest-2.2 O/E* mutant nematodes.
O   Representative lifespan assay of wt and *gas-1(fc21); cest-2.2 O/E* mutant animals grown on control (solid lines) and *cest-2.2* (dashed lines) RNAi bacteria from hatching.
P   Quantification of body area of 5-day-old wt, *gas-1(fc21)* and *gas-1(fc21); cest-2.2 O/E* mutant nematodes, normalized to wt (one-way ANOVA with the Tukey's multiple comparison test, *n* = 18–30 biological replicates).
Q   Locomotor activity (arbitrary unit) of 10-day-old wt, *gas-1(fc21)* and *gas-1(fc21); cest-2.2 O/E* mutants (one-way ANOVA with Dunnett's *post-hoc* correction, *n* = 8).
R   Number of pharyngeal pumps over 60 s of 5-day-old wt, *gas-1(fc21)* and *gas-1(fc21); cest-2.2 O/E* mutant nematodes (one-way ANOVA with the Tukey's multiple comparison test, *n* = 10 biological replicates).
S   Total number of eggs (left panel) and number of eggs laid each day (right panel) since hatching by wt, *gas-1(fc21)* and *gas-1(fc21); cest-2.2 O/E* mutant nematodes (ordinary one-way ANOVA with the Tukey's multiple comparisons test, *n* = 8–12 biological replicates).

Data information: In E, F, H, K, R, and S (left), mean ± SEM; in L, P, and Q, middle lines represents the median, and the upper and lower lines represent the upper and lower quartiles, respectively; in G, I, J, M, N, and O, the median lifespan ± SEM is reported underneath the graphs and additional information (e.g., *n* numbers) are reported in Appendix Table S1; in S (right) points indicate mean ± SEM. Across experiments, *P*-value summary is ns = not significant, *P < 0.05, **P < 0.01, ***P < 0.001, ****P < 0.0001.

conserved proteins (Fig 1D). One of these proteins is ZC376.2/ CEST-2.2, which is a carboxylesterase phylogenetically related to the serine hydrolase family and orthologous to human carboxylesterases and carboxyl ester lipases (Chen *et al*, 2019; Le *et al*, 2020). As recently described (Le *et al*, 2020), CEST-2.2 localizes to intestinal granules and contributes to the biosynthesis of ascarosides, including ascr#8, ascr#81, and ascr#82. Since CEST-2.2 is the most likely to play a role in metabolism, we decided to make this candidate the focus of our study. We performed quantitative real-time PCR (qRT-PCR) and confirmed that *cest-2.2* was downregulated in *gas-1(fc21)* mutants compared with wt animals, whereas it was upregulated in a H3.3-dependent manner in *nuo-6(qm200)* mutant nematodes (Figs 1E and EV1B). To test the role of *cest-2.2* in longevity, wt and *nuo-6* mutant nematodes were grown on bacteria expressing double-strand RNA against *cest-2.2*. We observed that *cest-2.2* RNAi inhibited *nuo-6(qm200)* longevity (Fig 1F and G and Appendix Table S1) as well as also slightly (yet significantly) reduced the survival of wt nematodes (Fig 1H and I, Appendix Table S1). To further explore CEST-2.2 contribution to survival, we ablated the *cest-2.2* encoding region using CRISPR/Cas9-based gene editing (Fig EV1C). We found that *cest-2.2 loss-of-function (lf)* mutants had a minor tendency toward a decreased median lifespan compared with wt animals, whereas *cest-2.2(lf)* inhibited the lifespan extension due to the RNAi against complex IV subunit CCO-1 (Figs 1J

and EV1D, Appendix Table S1). When we attempted to generate *nuo-6, cest-2.2* double mutants, we could obtain only hermaphrodites carrying the two mutant alleles in heterozygosity, further highlighting the contribution of CEST-2.2 to the survival of complex I-deficient nematodes. However, *cest-2.2* downregulation had no effect on the survival of long-lived *sod-2(ok1030)* and complex III *isp-1(qm150)* mutants (Fig EV1E and F, Appendix Table S1). Consistent with the metabolic heterogeneity of mitochondrial diseases (Lake *et al*, 2016; Wallace, 2018; Frazier *et al*, 2019; Russell *et al*, 2020), these data suggest that CEST-2.2 influences the lifespan of mitochondrial mutant nematodes depending on the genetic lesions in question.

Next, we reasoned that *cest-2.2* upregulation could ameliorate the survival of short-lived complex I mutants. We therefore generated a strain stably overexpressing CEST-2.2 (*cest-2.2 O/E*) by biolistic transformation. qRT-PCR showed a significant CEST-2.2 upregulation in our newly generated line compared with controls (Figs 1K and EV1G). Consistently, SureQuant-based targeted mass spectrometry using two unique CEST-2.2 peptides (LSTGTIEGR and HGEDFAYAFGTNR) revealed that our transgene could also restore CEST-2.2 protein levels when introduced in *gas-1(fc21)* mutants (Fig 1L and Appendix Table S2). We found that *cest-2.2 O/E* animals displayed a slight tendency toward lifespan extension compared with wt nematodes (Fig 1M and Appendix Table S1). Remarkably,

cest-2.2 O/E strongly stimulated the lifespan of short-lived complex I-deficient animals, with a median lifespan that was approximately 38% longer than that of *gas-1(fc21)* mutant nematodes (Fig 1N and Appendix Table S1). Both *cest-2.2* downregulation and *(lf)* mutation abrogated the lifespan extension of *gas-1(fc21); cest-2.2 O/E* mutant nematodes, while *cest-2.2* RNAi had no effect on *gas-1* survival (Figs 1N–O and EV1G–J, Appendix Table S1). These lifespan assays further emphasize that the increased survival is specifically linked to CEST-2.2 activity and not to other confounding effects (e.g., integration site of the transgene). Of note, *cest-2.2 O/E* had no influence on *nuo-6* lifespan, whereas it moderately extended the survival of complex II-deficient *mev-1* mutants (Fig EV1K and L, Appendix Table S1).

Phenotypically, we noticed that *cest-2.2 O/E* had negligible effect on body size and locomotory activity, although *cest-2.2(lf)* animals were larger than wt (Fig EV1M and N). Nevertheless, *cest-2.2 O/E* led to a significant increase in body size as well as to complete rescue of locomotory defects caused by the *gas-1(fc21)* lesion (Fig 1P and Q). Furthermore, *cest-2.2 O/E* did not alter the pharyngeal pumping rate and egg laying of *gas-1* mutants (Fig 1R and S), ruling out any confounding effect on survival due to fertility or food intake. Together, our findings show that CEST-2.2 overexpression shifts the survival threshold of complex I-deficient animals toward longevity.

CEST-2.2 O/E stimulates mitochondrial respiration in complex I-deficient nematodes

We next explored whether *cest-2.2 O/E* could influence mitochondrial bioenergetics in *gas-1(fc21)* nematodes. Using a previously adapted Seahorse protocol (Troulinaki *et al*, 2018; Gioran *et al*, 2019), we observed that *cest-2.2 O/E* was not sufficient to rescue the basal respiration defects of *gas-1* mutants; however, it did significantly increase their maximal respiration (Fig 2A–C), indicating that

the mitochondria of *gas-1; cest-2.2 O/E* animals possessed more metabolic flexibility, possibly due to an increased availability of substrates and tricarboxylic acid cycle (TCA) activity as shown in other biological contexts (van der Windt *et al*, 2012; Pfleger *et al*, 2015). The increased maximal respiration was associated with a visible trend toward more ATP levels in *gas-1; cest-2.2 O/E* animals compared with *gas-1* mutants (Fig 2D). As expected, *cest-2.2* RNAi almost abrogated the enhanced mitochondrial plasticity observed in *gas-1; cest-2.2 O/E* nematodes (Fig 2E and F). Both *cest-2.2 O/E* and *cest-2.2(lf)* animals had mitochondrial respiration profiles comparable to wt nematodes (Fig 2G), further indicating an exclusive effect on complex I-deficient mitochondria. We performed high-resolution confocal microscopy and observed that CEST-2.2 O/E was also sufficient to ameliorate the aberrant mitochondrial fragmentation in the gut of *gas-1* mutant nematodes (Fig 2H), indicating a better maintenance of the mitochondrial network. Remarkably, CEST-2.2 O/E counteracted mitochondrial fragmentation in the body wall muscle cells of *gas-1(fc21)* mutants (Fig 2I), indicating a beneficial effect across different tissues.

Since lifespan extension of mitochondrial mutants often depends on a transcriptional upregulation of defensive mechanisms (Lin & Haynes, 2016; Quirós *et al*, 2016; Riera *et al*, 2016; Shpilka & Haynes, 2018; Mottis *et al*, 2019), we set out to explore whether CEST-2.2 O/E could stimulate mitochondrial UPR (UPR^{mt}) and other stress response pathways involved in the detoxification of detrimental molecules, such as reactive oxygen species (ROS). To do so, we first assessed the expression of the *zcIs13[hsp-6p::gfp]* transgene, a widely accepted UPR^{mt} marker (Benedetti *et al*, 2006) under the transcriptional regulation of the bZip transcription factor ATFS-1 (Nargund *et al*, 2012). We found that *cest-2.2 O/E* significantly enhanced *zcIs13[hsp-6p::gfp]* expression in *gas-1* mutants (Fig 2J), suggesting that UPR^{mt} was strongly induced. Moreover, we observed that *atfs-1(lf)* did not modify the maximal respiration of *gas-1(fc21); cest-2.2 O/E* animals (Fig 2K and L). Of note, *cest-2.2*

Figure 2. CEST-2.2 O/E stimulates mitochondrial respiration in complex I-deficient nematodes.

A   Representative oxygen consumption rate (OCR) curve of 5-day-old wt, *gas-1(fc21)* and *gas-1(fc21); cest-2.2* O/E mutant nematodes as measured with a Seahorse XF24 Analyzer. Injection time of FCCP and NaN$_3$ is indicated with arrows (*n* = 9 biological replicates, from three independent experiments).

B, C   Indices of (B) normalized basal OCR and (C) maximal respiration of wt, *gas-1(fc21)* and *gas-1(fc21); cest-2.2* O/E mutant nematodes across (*n* = 9, one-way ANOVA with the Tukey's multiple comparison test, *n* = 9 biological replicates, from three independent experiments).

D   Relative ATP content of *gas-1(fc21)* and *gas-1(fc21); cest-2.2* O/E nematodes (unpaired *t*-test, *n* = 3 biological replicates).

E, F   Representative (E) Seahorse experiment and statistical analysis of (F) basal OCR and maximal respiration of 5-day-old *gas-1; cest-2.2 O/E* mutant *C. elegans* fed with control and *cest-2.2* RNAi since hatching (ordinary one-way ANOVA with the Tukey's multiple comparisons test, *n* = 7–9 biological replicates, from three independent experiments).

G   OCR profiles of wt, *cest-2.2 O/E* and *cest-2.2(lf)* nematodes upon sequential treatment with FCCP and NaN$_3$ (*n* = 9–10 biological replicates, from three independent experiments).

H   Representative images of control, *gas-1(fc21)* and *gas-1(fc21); cest-2.2 O/E* nematodes expressing mitochondria-targeted GFP in the intestine (scale bar = 5 μm).

I   Representative high-resolution confocal images of *C. elegans* expressing mitochondria-targeted GFP in the body wall muscle cells (scale bar = 10 μm). Quantification of mitochondrial morphology (elongation) is reported in the right panel (one-way ANOVA with Holm-Sidak's correction, *n* = 37–47 animals from three independent experiments).

J   Representative western blot analysis and densitometry of *zcIs13[hsp-6p::GFP]* expression in control, *gas-1(fc21)* and *gas-1(fc21); cest-2.2 O/E* animals (one-way ANOVA with Holm-Sidak's correction, *n* = 3 biological replicates).

K, L   Representative (K) Seahorse profile and (L) statistical analysis of basal OCR and maximal respiration of mutant nematodes (unpaired *t*-test, *n* = 12–13 biological replicates, from three independent experiments).

M   Immunoblot and statistical analysis of *zcIs13[hsp-6p::GFP]* expression in control and *nuo-6(qm200)* animals fed with empty vector (C RNAi) and *cest-2.2* RNAi bacteria (unpaired *t*-test, *n* = 3 biological replicates).

Data information: In A, E, G, K, points represent mean ± SEM; in B, C, D, F, J (right), L, and M (right), bars represent mean ± SEM; in I (right), middle line represents the median, and the upper and lower lines represent the upper and lower quartiles, respectively. Across experiments, *P*-value summary is ns = not significant, *P < 0.05, **P < 0.01, ***P < 0.001, ****P < 0.0001.
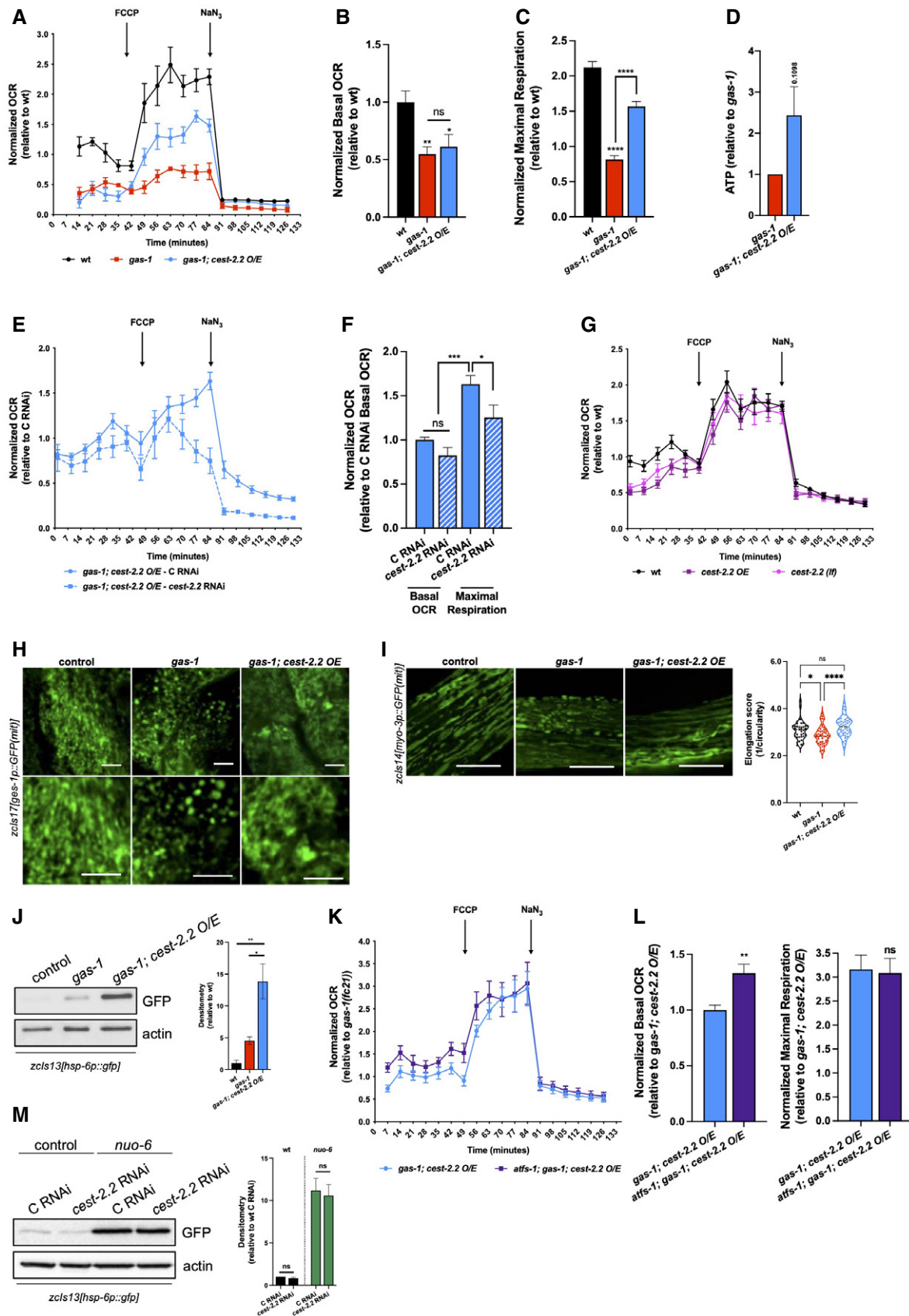
Figure 2.

downregulation was not sufficient to alter *zcIs13[hsp-6p::gfp]* expression in *nuo-6(qm200)* (Fig 2M), possibly because UPR^{mt} was already efficiently engaged at an early larval stage and before an efficient RNAi effect. We went on to measure the expression of SOD-3 and GST-4, two detoxifying enzymes that are transcriptionally regulated in response to oxidative stress. We found that genetic manipulation of *cest-2.2* did not alter *sod-3* and *gst-4* expression in neither *nuo-6* nor *gas-1* mutants (Fig EV2A–H), indicating that CEST-2.2 does not influence transcription factors targeting *sod-3* and *gst-4* promoters. To further rule out any role of oxidative stress on the observed lifespan extension, we exposed *gas-1; cest-2.2 O/E* animals to the free-radical scavenger ascorbate/vitamin C. Contrary to other long-lived mitochondrial mutants (Yang & Hekimi, 2010), vitamin C did not alter the survival of wt, *gas-1(fc21)* and *gas-1(fc21); cest-2.2 O/E* nematodes (Fig EV2I). Taken together, our data suggest that UPR^{mt} is engaged and may contribute to *gas-1; cest-2.2 O/E* stress resilience.

CEST-2.2 overexpression stimulates lipid metabolism in complex I-deficient *C. elegans*

We set out to investigate the biological processes underlying the lifespan extension of *gas-1; cest-2.2 O/E* mutants. To do so, we initially assessed the expression pattern of *cest-2.2* in *C. elegans* by generating a construct with the annotated sequence of the *cest-2.2* promoter and a GFP cassette. We obtained a *cest-2.2p::GFP* extrachromosomal array by microinjection and, consistent with previous evidence (Le *et al*, 2020), observed high GFP expression levels primarily in the intestine (Fig 3A). Given its hydrolytic activity as well as its discrete expression in one of the main tissues involved in the storage of lipids and other macromolecules (Lee *et al*, 2003; McKay *et al*, 2003), we reasoned that CEST-2.2 might have two functions: to drive fatty acid β-oxidation and/or to generate signaling molecules (Fig 3B), such as ascarosides (Ludewig & Schroeder, 2013). To rule out the lifespan-extending properties of the latter, we exposed *gas-1*

(fc21) nematodes to ethanol (as a control), ascr#8, and ascr#81. We performed confocal analysis and found that ascaroside treatments did not rescue mitochondrial fragmentation due to complex I deficiency (Fig 3C). Furthermore, ascr#8 treatment from hatching did not alter *gas-1(fc21)* survival (Fig 3D and Appendix Table S1).

To investigate CEST-2.2 biology in the context of mitochondrial dysfunction, we dissected adult intestines, extracted total RNA, and performed next-generation RNA sequencing (NGS). After confirming the higher expression of *cest-2.2* in *gas-1(fc21); cest-2.2 O/E* animals compared with wt and *gas-1(fc21)* mutant animals (Fig 3E), we analyzed our NGS data and found that 560 genes were differentially regulated in *gas-1(fc21)* compared to wt animals, 376 of which have either a known or putative function (Fig 3F and G and Appendix Table S3). As expected with intestinal tissue and consistent with our previous study (Gioran *et al*, 2019), most of these genes are specifically involved in metabolic processes (Fig 3H and Appendix Table S3). When we compared the transcriptional profiles of *gas-1 (fc21); cest-2.2 O/E* animals and *gas-1* mutants, we found that a total of 354 genes were significantly dysregulated (Fig 3F and G), with many of these encoding enzymes involved in lipid metabolism (Fig 3H). Ingenuity pathway analysis (IPA) predicted that *gas-1 (fc21)* animals had decreased fatty acid oxidation and, as a consequence, potential changes in stored fatty acids (Fig 3I). Together, our data indicate that *gas-1(fc21)* mutants have impaired fatty acid metabolism, whereas *gas-1(fc21); cest-2.2 O/E* nematodes may be able to mobilize more efficiently lipid stores and to induce lipid catabolism.

To experimentally support our NGS data-based IPA predictions, we initially explored eventual changes of whole body fat using an Oil Red O (ORO) staining. We found that *gas-1(fc21); cest-2.2 O/E* animals had significantly reduced lipid stores in the intestine when compared to both wt and *gas-1(fc21)* mutant nematodes (Fig 4A–F), further implying that *gas-1(fc21); cest-2.2 O/E* animals may have enhanced lipid catabolism as predicted by IPA (Fig 3I). There was no correlation between the ORO staining and body size (Fig 4D),

---

Figure 3. CEST-2.2 overexpression induces transcriptional changes in *gas-1* mutant nematodes.

A   Representative image of 5-day-old *cest-2.2p::GFP* (left panel) and an age-matched GFP-negative control (right panel). Scale bar = 100 μm.

B   Schematic representation of CEST-2.2 participation in very long-chain fatty acid (VLCFA) metabolism and ascaroside biosynthesis. Metabolites from peroxisomal β-oxidation may contribute to the biosynthesis of medium-chain fatty acid (1) and intracellular signaling (2). Ascarosides may take part in cell-autonomous and/or cell-nonautonomous signaling.

C   Confocal images of mitochondrial morphology in the intestines of *gas-1(fc21)* animals exposed to either 1.7% ethanol (control), 1 μM ascr#8 or 1 μM ascr#81 (scale bar= 5 μm).

D   Representative lifespan analysis of *gas-1(fc21)* animals exposed to ethanol (control) and 1 μM ascr#8 from hatching. Underneath is the average median lifespan ± SEM across replicates.

E   qRT-PCR of *cest-2.2* expression in the intestines of 5-day-old wt, *gas-1(fc21)*, *gas-1(fc21); cest-2.2 O/E* and *nuo-6(qm200)* animals (one-way ANOVA with the Tukey's multiple comparison test, *n* = 3 biological replicates).

F   Volcano plot of transcriptomes of intestines from *gas-1(fc21)* versus wt (left panel) and *gas-1(fc21); cest-2.2 O/E* versus *gas-1(fc21)* mutants (right panel). In red: significantly dysregulated genes (5% FDR).

G   Pie charts of differentially regulated genes in *gas-1(fc21)* versus wt (top panel) and *gas-1(fc21); cest-2.2 O/E* versus *gas-1(fc21)* mutants (bottom panel), showing proportion of genes of unknown function or involved in metabolism. Genes involved in lipid metabolism specifically represented in a small box within the metabolism slice.

H   Heatmap of genes involved in lipid metabolism in *gas-1(fc21)* versus wt and *gas-1(fc21); cest-2.2 O/E* versus *gas-1(fc21)*.

I   Ingenuity pathway analysis (IPA) of transcriptome in *gas-1(fc21)* versus wt (top panel) and *gas-1(fc21); cest-2.2* O/E versus *gas-1(fc21)* (bottom panel) with their predicted consequences on lipid metabolism. In red/green: results from the transcriptome. In blue/orange: IPA-generated predicted outcome of this gene dysregulation. Shades of red and green are proportional to log$_2$(fold change), while shades of blue and orange are proportional to the statistical strength of the prediction (*z*-score), as calculated by IPA.

Data information: In D, the median lifespan ± SEM is reported underneath the graphs and additional information (e.g., *n* numbers) are reported in Appendix Table S1; in E, points represent mean ± SEM. Across experiments, *P*-value summary is ns = not significant, *P < 0.05, **P < 0.01, ***P < 0.001, ****P < 0.0001.
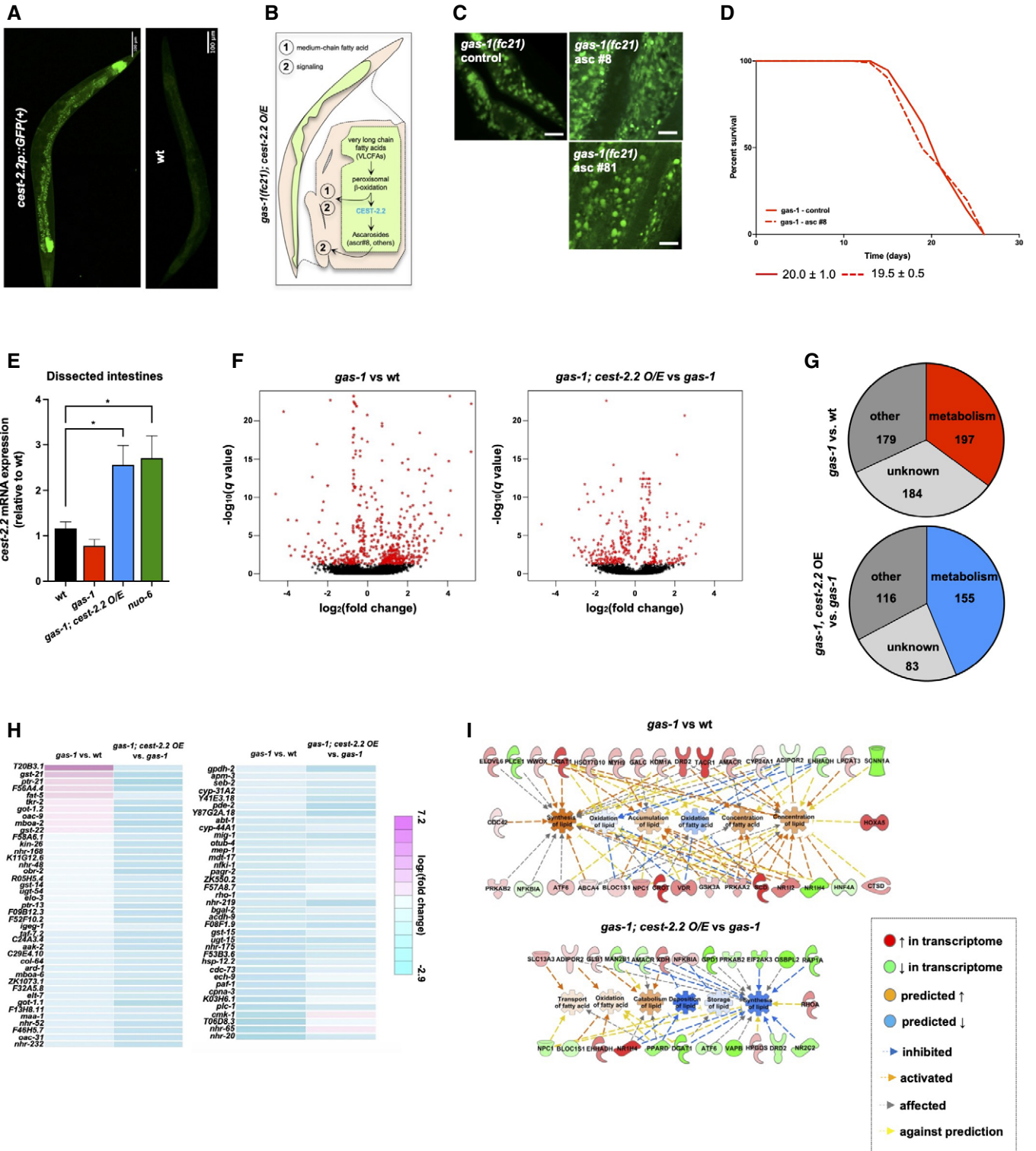
Figure 3.

ruling out the confounding effect of the larger body mass of *gas-1 (fc21); cest-2.2 O/E* animals (Fig 1P). As a side note, *cest-2.2 O/E* nematodes also had slightly less ORO staining in the hindgut when compared to wt ones (Fig 4E and F), though the effect was not as

pronounced as the effect of CEST-2.2 O/E in the context of complex I deficiency (Fig 4A–C). While the mean intensity of ORO staining was not significantly increased in *C. elegans* carrying *cest-2.2 (lf)* alleles, many animals did present with large, mislocalized lipid
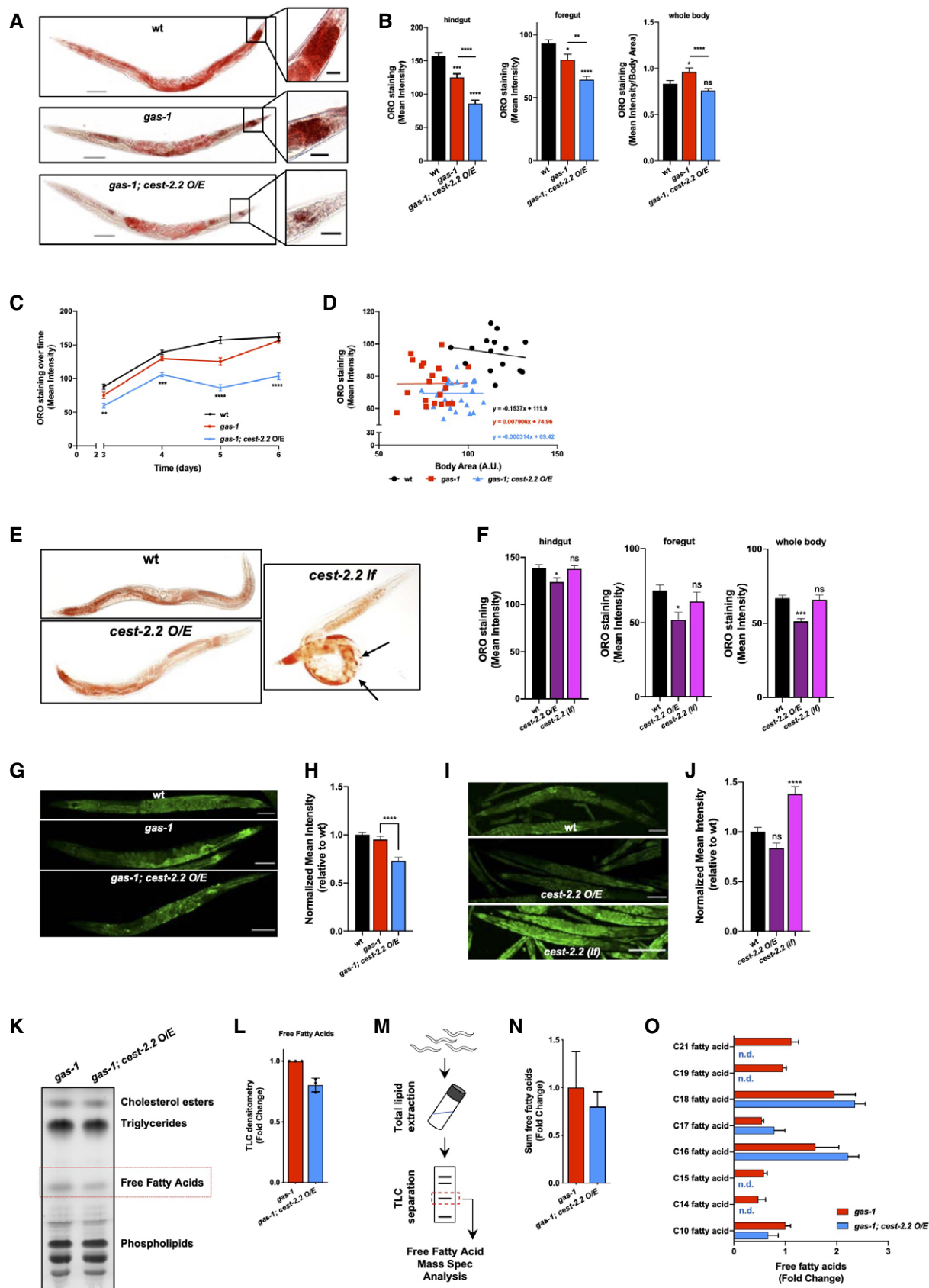
Figure 4.

Figure 4. CEST-2.2 overexpression modulates fat storage and lipid composition in *gas-1* mutant nematodes.

A Representative images of 5-day-old wt, *gas-1(fc21)* and *gas-1(fc21); cest-2.2 O/E* mutant animals stained with Oil Red O (ORO) (scale bar = full image-100 μm; hindgut magnification-20 μm).
B Quantification of hindgut (left panel), foregut (center panel), and whole body (right panel) of 5-day-old wt, *gas-1(fc21)* and *gas-1(fc21); cest-2.2 O/E* mutant nematodes stained with ORO (one-way ANOVA with the Tukey's multiple comparison test, *n* = 18–26 animals).
C Quantification of mean intensity of ORO staining in the hindgut of wt, *gas-1(fc21)* and *gas-1(fc21); cest-2.2 O/E* mutant nematodes at different time points, starting from L4 stage (one-way ANOVA with Dunnett's *post-hoc* correction, *n* = 18–26 animals).
D Mean intensity of ORO staining in the whole body of 5-day-old wt, *gas-1(fc21)* and *gas-1(fc21); cest-2.2 O/E* mutant nematodes plotted against body area.
E Representative images of wt, *cest-2.2 O/E* and *cest-2.2 (lf)* animals stained with ORO. Arrows indicate mislocalized lipid droplets.
F Quantification (mean intensity ± SEM) of ORO staining in hindgut (left panel), foregut (center panel), and whole body (right panel) of 5-day-old nematodes (one-way ANOVA with Dunnett's *post-hoc* correction, *n* = 11–17 animals).
G Representative images of 5-day-old wt, *gas-1(fc21)* and *gas-1(fc21); cest-2.2 O/E* mutant animals stained with LipidTOX (scale bar = 100 μm).
H Statistical analysis of whole body LipidTOX intensity of 5-day-old nematodes (ordinary one-way ANOVA with the Tukey's multiple comparison test, *n* = 25–37 animals).
I, J Representative images of nematodes stained with LipidTOX (I) (scale bar = 100 μm), with quantification (J) (mean intensity ± SEM) of LipidTOX staining.
K Representative thin layer chromatography (TLC) plate of samples from 5-day-old *gas-1(fc21)* and *gas-1(fc21); cest-2.2 O/E* mutant nematodes.
L Densitometry of TLC-separated free fatty acids (FFA) across three biological replicates in 5-day-old mutant animals.
M Schematic representation of free fatty acid mass-spec analysis.
N Sum of TLC-separated FFA of 5-day-old animals (*n* = 5 biological replicates).
O Quantification of individual FFA detected after TLC separation in 5-day-old *gas-1(fc21)* and *gas-1(fc21); cest-2.2 O/E* mutant nematodes (*n* = 5 biological replicates, n.d. = not detected).

Data information: In B, F, H, J, L, N, and O, bars represent mean ± SEM; in C, points represent mean ± SEM. Across experiments, *P*-value summary is ns = not significant, *$P < 0.05$, **$P < 0.01$, ***$P < 0.001$, ****$P < 0.0001$.

droplets (Fig 4E), as well as having a significantly larger body size when compared to wt nematodes (Fig EV1M). To further support our lines of evidence, we stained nematodes with the neutral lipid stain LipidTOX Green (Klapper *et al*, 2011) and observed that *cest-2.2 O/E* animals had a tendency toward less lipids as shown by the ORO staining (Fig 4G–J). Of note, *cest-2.2 (lf)* exhibited more LipidTOX Green staining compared with wt (Fig 4I and J). Furthermore, we noticed that *cest-2.2* downregulation in *nuo-6* mutant animals also resulted in a significant increase in LipidTOX staining (Fig EV3A and B). Together, these findings indicate that CEST-2.2 O/E can influence lipid deposits in both wt and complex I-deficient nematodes.

It is known that lipid-rich particles are used to synthesize yolk particles in the intestine that are then transferred to developing oocytes (Kimble & Sharrock, 1983; Perez & Lehner, 2019; Chen *et al*, 2020). However, *gas-1(fc21); cest-2.2 O/E* and *gas-1(fc21)* had a comparable ORO staining in gonads and eggs (Fig EV3C), which rules out an increased lipid transfer to produce viable progeny. Since vitellogenin proteins have lipid transporter activity and mobilize lipids during starvation (Harvald *et al*, 2017), we further explored this biological aspect and assessed genes associated with yolk production. We found that vitellogenin genes were not differentially regulated in *gas-1(fc21); cest-2.2 O/E* mutants compared with *gas-1(fc21)* (Fig EV3D). Moreover, while *vit-1* downregulation slightly extended *C. elegans* lifespan (Fig EV3E and Appendix Table S1) as previously described (Seah *et al*, 2016), *vit-1* deficiency had no effect on *gas-1(fc21)* survival and robustly reduced the lifespan extension of *gas-1(fc21); cest-2.2 O/E* mutants (Fig EV3E and Appendix Table S1). Together, these data support the hypothesis that *gas-1(fc21); cest-2.2 O/E* animals have less lipid stores because of enhanced lipid catabolism, rather than as a consequence of a preferential nutrient transferring to the developing progeny.

To identify individual lipid species and gain knowledge of the underling molecular processes, we set off to refine our studies using more quantitative methods. Because wt animals lay significantly

more eggs than *gas-1(fc21)* and *gas-1(fc21); cest-2.2 O/E* (Fig 1S), we excluded them from further lipid analysis to avoid the confounding effect of fat stores in the developing embryos. First, we performed a qualitative thin layer chromatography (TLC) in samples from *gas-1(fc21)* and *gas-1(fc21); cest-2.2 O/E* animals (Fig 4K). Among all the detected lipids, our TLC analysis showed that free fatty acids (FFAs) tended to be less in *cest-2.2 O/E* animals (Fig 4K and L). We then performed a quantitative mass-spec analysis of FFAs and found comparable FFA levels between *gas-1(fc21)* and *gas-1(fc21); cest-2.2 O/E* animals (Fig 4M and N). However, further investigation of the individual FFAs showed that, compared to *gas-1(fc21)* mutants, *gas-1(fc21); cest-2.2 O/E* animals had a dramatically altered FFA composition with undetectable levels of C-14, C-15, C-19, and C-21 fatty acids (Fig 4O). Of note, total lipid content was comparable between *gas-1(fc21)* and *gas-1(fc21); cest-2.2 O/E* animals, with only a handful of fatty acids that were slightly altered (Fig EV3F and G), possibly due to the confounding effect of the plentiful lipids present in cell membranes. Overall, these results strongly indicate that CEST-2.2 O/E alters stored lipid composition, stimulating the mobilization of certain FFAs in complex I-deficient animals.

CEST-2.2 overexpression stimulates lifespan via fatty acid beta-oxidation

Our multiomics indicated that CEST-2.2 can influence lipid deposits by enhancing fat catabolism. Consistent with our IPA predictions (Fig 3I), we found that key enzymes involved in lipid metabolism were upregulated in *gas-1(fc21); cest-2.2 O/E* animals compared with *gas-1(fc21)* mutants (Fig 5A and B). Since these are described targets of nuclear hormone receptors NHR-49 and NHR-80 (Van Gilst *et al*, 2005; Brock *et al*, 2006), we performed epistatic analyses of animals grown on double-strand RNA against either *nhr-49* or *nhr-80*. We found that *nhr-49* downregulation significantly decreased the survival of *gas-1(fc21); cest-2.2 O/E*
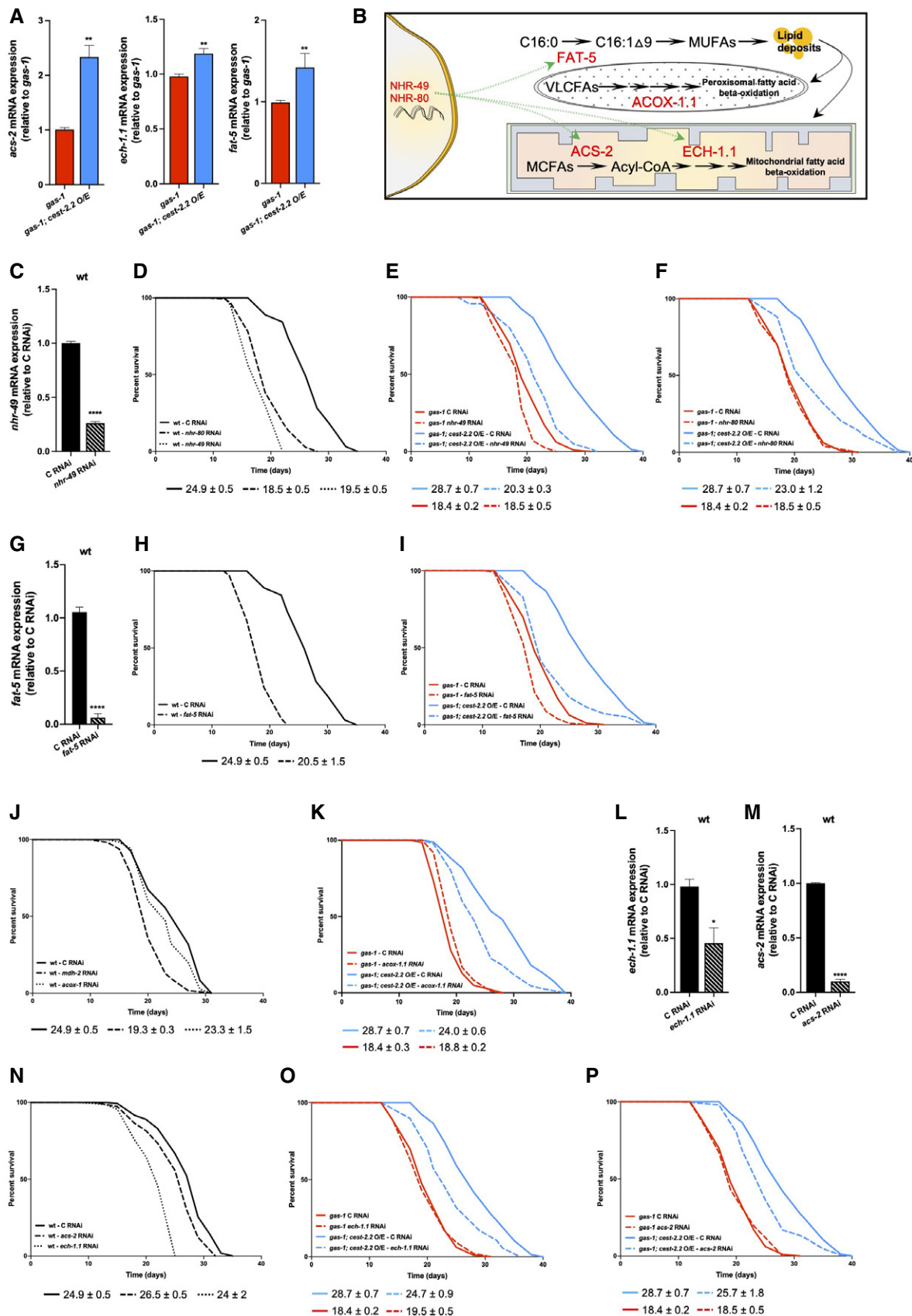
Figure 5.

Figure 5. Lifespan extension of *cest-2.2 O/E* animals requires NHR-49, NHR-80, and their downstream targets.

A   qRT-PCR of *acs-2*, *ech-1.1*, and *fat-5* mRNA expression in 5-day-old mutant nematodes (Mann–Whitney *U* test, *n* = 6 biological replicates).
B   Simplified schematic of NHR-49/NHR-80 participation to fatty acid beta-oxidation. Green dotted arrows indicate potential transcriptional regulation by NHR-49/ NHR-80. In red, enzymes have been tested in our epistatic analysis. MUFAs is monounsaturated fatty acids, VLCFAs indicates very long chain fatty acid, and MCFAs is medium-chain fatty acid.
C   qRT-PCR of *nhr-49* expression in wt nematodes grown on control and *nhr-49* RNAi expressing bacteria (unpaired *t*-test, *n* = 3 biological replicates).
D   Lifespan assay of wt nematodes exposed to control, *nhr-80* and *nhr-49* RNAi.
E, F   Representative survival curves of *gas-1(fc21)* and *gas-1(fc21); cest-2.2 O/E* nematodes grown (E) control versus *nhr-49* RNAi and (F) control versus *nhr-80* RNAi.
G   qRT-PCR of *fat-5* mRNA expression in wt nematodes grown on control and *fat-5* RNAi expressing bacteria (unpaired *t*-test, *n* = 3 biological replicates).
H, I   Lifespan assay of (H) wt and (I) *gas-1(fc21)* versus *gas-1(fc21); cest-2.2 O/E* nematodes grown on control and *fat-5* RNAi bacteria.
J, K   Representative survival curves of (J) wt and (K) *gas-1(fc21)* versus *gas-1(fc21); cest-2.2 O/E* nematodes fed with control and RNAi against *mdh-2* (for wt) and *acox-1.1*.
L, M   qRT-PCR of (L) *ech-1.1*- and *acox-1.1*-deficient (M) *acs-2* mRNA expression in wt nematodes grown on control and RNAi expressing bacteria (unpaired *t*-test, *n* = 3 biological replicates).
N–P   Lifespan assays of (N) wt and (O-P) *gas-1(fc21)* versus *gas-1(fc21); cest-2.2 O/E* mutant nematodes grown on control, *ech-1.1* and *acs-2* RNAi expressing bacteria.

Data information: In A, C, G, L, and M, bars represent mean ± SEM; in D, E, F, H, I, J, K, N, O, and P, the median lifespan ± SEM across replicates is reported underneath the graphs, and additional information (e.g., *n* numbers) is reported in Appendix Table S1. Certain lifespans were run at the same time, but representative figures were split for the sake of clarity (i.e., panels E, F, I, O, and P come from the same experiment; panels D and H come from the same experiment—see Appendix Table S1). Across experiments, *P*-value summary is **P* < 0.05, ***P* < 0.01, ****P* < 0.001, *****P* < 0.0001.

animals (Fig 5C–E and Appendix Table S1). Downregulation of *nhr-49* did not affect the median lifespan of *gas-1(fc21)* mutants, although it reduced their maximal lifespan (Fig 5E and Appendix Table S1). Consistently, *nhr-80* deficiency also inhibited the survival of *gas-1(fc21); cest-2.2 O/E* nematodes without affecting the median lifespan of *gas-1(fc21)* mutants (Fig 5F and Appendix Table S1). To our surprise and in contrast to previous evidence (Brock *et al*, 2006), both *nhr-49* and *nhr-80* RNAi had an impact on wt lifespan (Fig 5D and Appendix Table S1). These data suggest that CEST-2.2 extends *gas-1(fc21)* lifespan by engaging NHR-49- and NHR-80-dependent pathways.

The delta-9 fatty acid desaturase FAT-5 contributes to the biosynthesis of monounsaturated fatty acids (MUFAs) from palmitic acid (16:0) mostly coming from *E. coli* digestion (Brock *et al*, 2006, 2007; Watts & Ristow, 2017). Although *fat-5* deficiency can be partially compensated by *fat-6* expression because of functional redundancy of delta-9 desaturases in *C. elegans* (Brock *et al*, 2006), we found that *fat-5* downregulation significantly compromised the lifespan extension of *gas-1(fc21); cest-2.2 O/E* nematodes and partially reduced *gas-1(fc21)* survival (Fig 5G–I and Appendix Table S1). The lifespan reduction was associated with an increased LipidTOX staining (Fig EV4A), suggesting that loss of FAT-5-dependent fatty acid biosynthesis undermines the lifespan-extending properties of CEST-2.2 because of the inability to efficiently mobilize fatty acid content stored in the intestine. To challenge this hypothesis, we assessed the contribution of fatty acid beta-oxidation, knowing that short chain fatty acid oxidation occurs primarily in mitochondria, whereas longer fatty acids are usually oxidized in peroxisomes (Watts & Ristow, 2017). Since C-21 and C-19 fatty acids were not detected in our quantitative mass-spec analysis of FFAs (Fig 4O), we initially focused on the peroxisomal acyl-CoA oxidase ACOX-1/ ACOX1. We found that *acox-1* downregulation significantly reduced the lifespan of *gas-1(fc21); cest-2.2 O/E* animals, while having only a slight effect on the survival of wt nematodes (Fig 5J and aK and Appendix Table S1). We then downregulated the expression of mitochondrial acyl-CoA synthetase family member 2 ACS-2/ACSF2 and enoyl-CoA hydratase ECH-1.1/HADHA, both significantly upregulated in *gas-1(fc21); cest-2.2 O/E* mutants compared with *gas-1*

(fc21) animals (Fig 5A). We observed that downregulation of both *acs-2* and *ech-1.1* led to a partial lifespan reduction of *gas-1(fc21); cest-2.2 O/E* and wt animals, whereas the survival of *gas-1(fc21)* mutants remained unaffected (Fig 5L–P and Appendix Table S1). Together, these epistatic analyses suggest that fatty acid beta-oxidation is required for the lifespan extension of *gas-1(fc21); cest-2.2 O/E* mutants.

Oxaloacetate levels correlate with complex II- and LET-721/ ETFDH-dependent mitochondrial respiratory capacity of *gas-1 (fc21); cest-2.2 O/E* mutants

Our data indicate that CEST-2.2 overexpression can stimulate *gas-1 (fc21)* lifespan extension and the associated mitochondrial plasticity (Figs 1N and 2A–C), despite the inherited genetic lesion of complex I. To better understand the correlation between longevity and mitochondrial bioenergetics, we downregulated *nhr-49* and *nhr-80* in nematodes and measured OCR. Consistent with their essential role in survival (Fig 5D and E), we found that NHR-49 and, to a lesser extent, NHR-80 expression was required for the proper mitochondrial respiratory profiles of wt, *gas-1(fc21)* and *gas-1(fc21); cest-2.2 O/E* animals (Fig 6A–C).

It is assumed that mitochondrial respiratory capacity is a phenomenon linked to fatty acid beta-oxidation and to an enhanced efficiency in NADH and $FADH_2$ oxidation, which may be in part due to the ETC forming higher order respiratory supercomplexes (Brand & Nicholls, 2011; van der Windt *et al*, 2012; Calvo *et al*, 2020; Bertan *et al*, 2021). Since oxaloacetate is required to sustain the tricarboxylic acid (TCA) cycle and the oxidation of carbon units generated during fatty acid beta-oxidation (Fig 6D), we tested the consequence of oxaloacetate depletion by growing animals on RNAi expressing bacteria against malate dehydrogenase MDH-2. We found that *mdh-2* downregulation reduced the brood size and the lifespan extension of *gas-1(fc21); cest-2.2 O/E* nematodes, while having a moderate effect on wt survival (Figs 5J, 6E and EV4B, Appendix Table S1). Of note, *mdh-2* RNAi partially extended the lifespan of *gas-1(fc21)* mutants (Fig 6E and Appendix Table S1), possibly because of complete germline loss (Fig EV4C), which can occur as a consequence

Figure 6.

Figure 6. CEST-2.2 O/E requires oxaloacetate biosynthesis to support complex II- and LET-721/ETFDH-dependent mitochondrial respiration in *gas-1* mutants.

A–C   Statistical analysis of Seahorse basal OCR and maximal respiration of (A) wt, (B) *gas-1(fc21)* and (C) *gas-1(fc21); cest-2.2 O/E* nematodes fed with empty vector (C RNAi), *nhr-49* or *nhr-80* RNAi (ordinary one-way ANOVA with the Dunnett's multiple comparisons test, *n* = 4–12 biological replicates from three independent experiments).

D   Scheme of oxaloacetate biosynthesis. MDH-2 stimulates oxaloacetate biosynthesis, which can be used to support tricarboxylic acid cycle (TCA) and/or cytosolic phosphoenolpyruvate generation by PCK-1. In physiological settings, phosphoenolpyruvate can be used to generate pyruvate, which can be reduced to lactate or oxidized to acetyl-CoA (dashed lines).

E   Lifespan assay of nematodes exposed to control or *mdh-2* RNAi bacteria.

F, G   Representative Seahorse experiment (F) and maximal respiration (G) of untreated- and 24-h oxaloacetate-treated adult *gas-1(fc21)* nematodes (unpaired *t*-test, *n* = 9–10 biological replicates from three independent experiments).

H   Representative lifespan analysis of wt, *gas-1(fc21)* and *gas-1(fc21); cest-2.2 O/E* mutant animals exposed to control and *pck-1* dsRNA.

I, J   Representative OCR of 5-day-old *gas-1(fc21); cest-2.2 O/E* nematodes grown on control (C RNAi, solid lines) and *meu-1* RNAi (dashed lines) (I) and quantification of normalized basal OCR and maximal respiration (J) (ordinary one-way ANOVA with the Tukey's multiple comparisons test, *n* = 7–8 biological replicates from two independent experiments).

K   qRT-PCR of *let-721* mRNA expression in wt nematodes grown on control and RNAi expressing bacteria (*n* = 2 biological replicates).

L–N   Normalized OCR of (L) *gas-1(fc21)* and (M-N) *gas-1(fc21); cest-2.2 O/E* nematodes fed with control and RNAi expressing bacteria (one-way ANOVA with the Tukey's multiple comparison test, *n* = 5–8 biological replicates from two independent experiments).

O   Schematic representation of the proposed mechanism. In *gas-1* mutants, aberrant complex I impairs the proper ETC function, resulting in diminished mitochondrial respiration. Overexpression of CEST-2.2 stimulates fatty acid beta-oxidation, which promotes TCA cycle and the transferring of electrons to ubiquinone/coenzyme Q through complex II and LET-721/ETFDH. This ultimately contributes to electron transport maintenance and ATP production.

Data information: In A, B, C, G, J, K, L, and N, bars represent mean ± SEM; in E and H, the average median lifespan ± SEM across replicates is reported underneath the graphs, and additional information (e.g., *n* numbers) are reported in Appendix Table S1; in F, I, and M, points represent mean ± SEM. Across experiments, *P*-value summary is ns=not statistical, *$P < 0.05$, **$P < 0.01$, ***$P < 0.001$, ****$P < 0.0001$. Lifespans in panels E and H come from the same experiment, although they are represented separately for the sake of clarity (see Appendix Table S1).

of TCA cycle impairment (Rahman *et al*, 2014). Given the well-described lifespan-extending properties of germline loss in *C. elegans* (Arantes-Oliveira *et al*, 2002; Wang *et al*, 2008), it is likely that *mdh-2* RNAi extended the lifespan of *gas-1(fc21)* mutants due to this secondary effect. Of note, CEST-2.2 O/E partially preserved the germline and egg production of *gas-1(fc21)* mutants grown on *mdh-2* RNAi bacteria (Fig EV4C). In line with our hypothesis, oxaloacetate supplementation to *gas-1(fc21)* was sufficient to potentiate mitochondrial respiration (Figs 6F and G and EV4D and E), whereas feeding of the NAD$^+$-precursor nicotinamide mononucleotide (NMN) had no effect (Fig EV4F).

It is known that oxaloacetate can be used to synthesize phosphoenolpyruvate (Fig 6D), which may be redirected to generate glucose or lactate, the latter deriving from NADH-dependent pyruvate reduction. To test this hypothesis, we downregulated the expression of phosphoenolpyruvate carboxykinase 1 PCK-1/PCK1 (Fig EV4G), a key enzyme that converts cytosolic oxaloacetate into phosphoenolpyruvate. We found that *pck-1* silencing had a negligible effect on *gas-1(fc21); cest-2.2* O/E animals (Fig 6H and Appendix Table S1). Together, these data suggest that MDH-2 is required to support oxaloacetate for TCA cycle, rather than phosphoenolpyruvate biosynthesis, in *gas-1(fc21); cest-2.2 O/E*.

To gain further biological understanding of the enhanced mitochondrial respiratory capacity exhibited by *gas-1(fc21); cest-2.2 O/E*, we set up additional Seahorse experiments and explored the contribution of complex II, knowing that acetyl-CoA is condensed with oxaloacetate to be then oxidized via the TCA cycle. We found that *mev-1* downregulation significantly diminished the mitochondrial respiratory capacity in wt, *gas-1(fc21)* and *gas-1(fc21); cest-2.2 O/E* animals (Figs 6I and J, and EV4H and I), further highlighting the importance of complex II in the flexibility of mitochondrial bioenergetics (Brand & Nicholls, 2011; van der Windt *et al*, 2012). Next, we assessed the importance of transfer flavoprotein (ETF) and electron transfer flavoprotein dehydrogenase (ETFDH), which functionally couple fatty acid beta-oxidation to the ETC by transferring electrons from FADH$_2$ to ubiquinone/coenzyme Q (Eaton, 2002; Wang *et al*, 2019). While downregulation of LET-721/ETFDH did not alter the Seahorse profile of *gas-1(fc21)* mutants, it significantly reduced the maximal respiration of *gas-1(fc21); cest-2.2 O/E* nematodes (Fig 6K–N). Taken together, our data suggest that CEST-2.2 stimulates mitochondrial bioenergetics by shuttling electrons to complex II and LET-721/ETFDH (Fig 6O).

Discussion

Here, we report a genetic manipulation that transforms short-lived *gas-1(fc21)* nematodes into long-lived ones. Moreover, we describe how the usage of lipid deposits can be redirected to generate metabolites and reducing equivalents that stimulate the residual mitochondrial respiration despite an intrinsic complex I lesion.

Building up from our previous studies (Piazzesi *et al*, 2016; Gioran *et al*, 2019), we assessed the epigenetic landscapes of two models of complex I deficiencies that differently affect *C. elegans* lifespan. Specifically, we compared histone H3.3 deposition at the promoters of transcriptionally dysregulated genes in long-lived *nuo-6(qm200)* mutants and short-lived *gas-1(fc21)* animals. We herein report that H3.3 is indeed differentially loaded on promoters in short-lived and long-lived mitochondrial mutants, indicating that H3.3 deposition can be affected by the disease state of the organism. We found that H3.3 deposition on *cest-2.2* promoter correlates with its expression levels in *gas-1(fc21)* and *nuo-6(qm200)* mutants. We ultimately show that the recently described carboxylesterase CEST-2.2 influences the survival threshold of complex I-deficient nematodes, since it balances potentially deleterious mitochondrial lesions by engaging catabolic pathways that enable the usage of alternative resources to generate energy and sustain longevity. In this regard, our NGS data in *gas-1* mutants demonstrate that CEST-2.2 O/E

stimulates the regulation of genes that are primarily involved in lipid mobilization and catabolism, whereas it suppresses the accumulation of storage lipids.

The contribution of lipid metabolism in age-related processes has attracted much attention because of its relevance in human illnesses (Johnson & Stolzing, 2019). In the context of aging, a tightly regulated lipid mobilization can sustain lifespan-extending programs by coupling reproduction, energy availability, and somatic aging (Wang et al, 2008). Some of these events may be transgenerationally inherited, since they depend on chromatin remodeling and require an epigenetically regulated transcription of enzymes involved in the accumulation of distinct classes of lipids (e.g., MUFAs) (Greer et al, 2011; Han et al, 2017). In this regard, lipolysis is often an adaptive response to environment changes and nutritional state that may influence energy homeostasis and, as a consequence, longevity (O'Rourke & Ruvkun, 2013). Interestingly, lipid remodeling in distinct tissues may even have a paracrine function, since it induces cell-nonautonomous signals that promote epigenetic regulation of transcriptionally controlled prolongevity pathways (Imanikia et al, 2019; Schmeisser et al, 2019). In our work, we demonstrate that CEST-2.2 expression sustains the longevity of nuo-6 (qm200) nematodes and, more importantly, is sufficient to improve the survival of sick mitochondrial gas-1 mutants. The significant lifespan extension of gas-1(fc21); cest-2.2 O/E animals further emphasizes the essential nature of this tissue-specific hydrolase in the mobilization of available resources that can counteract mitochondrial lesions. With the recently acquired knowledge that CEST-2.2 is involved in very long-chain fatty acid oxidation and ascarosides biosynthesis (Le et al, 2020), we suggest that an increase of lipolysis and/or fatty acid beta-oxidation seems to provide an optimal trade-off between energy production and long-term stress. In support of this scenario, our epistatic analysis demonstrates that downregulation of key enzymes involved in lipid catabolism either partially or completely ablated the lifespan extension of gas-1(fc21); cest-2.2 O/E animals. Our current experimental evidence indicates that malate dehydrogenase MDH-2/MDH significantly supports the lifespan extension of gas-1(fc21); cest-2.2 O/E animals, while PCK-1/PCK1 contribution is negligible. Thus, it seems plausible that MDH-2/MDH is required to maintain levels of oxaloacetate that are compatible with an enhanced TCA cycle, which mediates the oxidation of carbon units deriving from fatty acid beta-oxidation. In support of this, downregulation of complex II subunit MEV-1 as well as LET-721/ETFDH disrupts the flexibility of mitochondrial bioenergetics acquired by CEST-2.2 overexpression. Based on these lines of experimental evidence, we propose that the available lipids are directed to generate acetyl-CoA that, upon condensation with oxaloacetate, is oxidized via TCA cycle to generate reducing equivalents that subsequently feed into the ETC through complex II and LET-721/ETFDH, thereby partially overcoming the intrinsic complex I defects. While this CEST-2.2-dependent metabolic rewiring is sufficient for complex I-deficient gas-1 and nuo-6 mutants, it has a much more modest effect in cco-1 silenced animals and no consequence in other mitochondrial mutants, such as sod-2 and isp-1. These findings indicate that lipid mobilization may represent a novel intervention for diseases associated with complex I defects, whereas it may be less attractive for genetic lesions affecting other respiratory complexes, further emphasizing the heterogenous nature of disease associated with mitochondrial dysfunction.

The "phenotypic threshold effect" is a multifactorial phenomenon that tries to explain the complex pathobiology of mitochondrial diseases (Rossignol et al, 2003). Based on this theory, clinical outcomes become evident when the existing compensatory mechanisms, which were initially sufficient to buffer mitochondrial deficiency, cannot longer satisfy extraordinary energy demands or sustain an additional environmental pressure. The subsequent energy crisis overcomes the established adaptation and triggers an irreversible cascade of detrimental events that eventually lead to pathology onset. In this complex scenario, it may appear counterintuitive that mild mitochondrial deficiency during development can stimulate C. elegans survival and healthspan (Lakowski & Hekimi, 1996; Felkai et al, 1999; Dillin et al, 2002; Rea et al, 2007; Riera et al, 2016; Shpilka & Haynes, 2018). This evidence further emphasizes the capacity of a biological system to adjust its metabolic activities adequately to overcome the lack of an efficient ATP generation primarily based on aerobic OXPHOS. To establish processes that promote stress resilience and longevity, cells must stimulate mitochondria-to-nucleus stress signaling that efficiently builds up an adaptive resistance to a potentially lethal metabolic state as well as to other detrimental insults, such as poor nutritional conditions and hostile environmental challenges. In our study, we show that CEST-2.2 overexpression specifically induces UPR^{mt}, indicating that the transcriptional engagement of distinct longevity pathways, rather than others (e.g., ROS-dependent signaling), may act as powerful disease modifiers.

Taken together, our findings imply that metabolic flexibility contributes to the phenotypic threshold effect observed in invertebrates carrying mitochondrial complex I lesions. As an added value, our study suggests that stimulation of lipid mobilization, through a transcriptionally regulated expression of a distinct intestine-specific hydrolase, is sufficient to circumvent complex I deficiency in C. elegans, with beneficial consequence on survival.

Materials and Methods

ATP quantification

Synchronized nematodes (100 mg) were collected, flash-frozen in liquid nitrogen and stored at −80°C. Pellets were homogenized in ATP buffer and deproteinized in 4 M perchloric acid and 2 M KOH as per the manufacturer's instructions (abcam ATP Assay Kit ab83355). Relative ATP content was measured with a microplate fluorescence reader at Ex/Em 535/587.

Caenorhabditis elegans strains and maintenance

All experiments were conducted at 20°C, and all strains were cultured following standard methods. The following strains were used in this study: wild-type N2 (Bristol), BAN125 gas-1(fc21)X; zuIs178[his-72p::his-72::GFP], BAN126 zuIs178[his-72p::his-72::GFP], BAN129 nuo-6(qm200)I; zuIs178[his-72p::his-72::GFP], BAN141 nuo-6(qm200)I; his-72(tm2066)III;his-71(ok2289)X, BAN150 gas-1 (fc21); zcIs13[hsp-6p::GFP; lin-15(+)], BAN198 unc-119(ed3)III, BAN328 unc-119(ed3)III; bonIs45[cest-2.2p::cest-2.2; unc-119(+)], BAN329 unc-119(ed3)III; gas-1(fc21)X; bonIs45[cest-2.2p::cest-2.2; unc-119(+)], BAN332 nuo-6(qm200); zcIs13[hsp-6p::GFP; lin-15(+)],

BAN335 *bonEx49[cest-2.2p::GFP myo-2p::mCherry]*, BAN351 *cest-2.2 (bon52)V*, BAN363 *gas-1(fc21)X; zcIs17[ges-1p::GFP(mit)]*, BAN366 *gas-1(fc21); zcIs14[myo-3p::GFP(mit)]*, BAN367 *unc-119(ed3)III; gas-1(fc21)X; bonIs45[cest-2.2p::cest-2.2; unc-119(+)], ges-1p::GFP(mit)*, BAN455 *unc-119(ed3)III; cest-2.2(bon52)V; gas-1(fc21)X; bonIs45 [cest-2.2p::cest-2.2; unc-119(+)]*, BAN466 *nuo-6(qm200)I; unc-119 (ed3)III; bonIs45[cest-2.2p::cest-2.2; unc-119(+)]*, BAN480 *mev-1 (kn1)III; unc-119(ed3)III; bonIs45[cest-2.2p::cest-2.2; unc-119(+)]*, BAN485 *unc-119(ed3)III; gas-1(fc21)X; bonIs45[cest-2.2p::cest-2.2; unc-119(+); zcIs13[hsp-6p::GFP; lin-15(+)]III*, BAN490 *unc-119(ed3)III; gas-1(fc21)X; bonIs45[cest-2.2p::cest-2.2; unc-119(+)]; zcIs14[myo-3p::GFP(mit)]*, BAN499 *unc-119(ed3)III; atfs-1(tm4525); gas-1(fc21) X; bonIs45[cest-2.2p::cest-2.2; unc-119(+)]*, CW152 *gas-1(fc21)X*, MQ887 *isp-1(qm150)IV*, MQ1333 *nuo-6(qm200)I*, RB1072 *sod-2 (ok1030)I*, SJ4100 *zcIs13[hsp-6p::GFP; lin-15(+)]*, SJ4103 *zcIs14[myo-3p::GFP(mit)]*, SJ4143 *zcIs17[ges-1p::GFP(mit)]*, and TK22 *mev-1 (kn1)III*. Some strains were provided by the CGC, which is funded by NIH Office of Research Infrastructure Programs (P40 OD010440).

ChIP-Seq

Chromatin extraction and chromatin immunoprecipitation followed by MeDIP sequencing (ChIP-Seq) was performed by Active Motif Inc using a previously validated antibody against GFP. L4 nematodes were collected in M9, flash-frozen in liquid nitrogen, and stored at −80°C. Chromatin was extracted as previously described (Askjaer *et al*, 2014). Approximately 10 μg of chromatin was then used for immunoprecipitation with 5 μl of a ChIP-validated rabbit polyclonal anti-GFP antibody (Abcam, ab290, Lot No. GR278073-1). Sequence reads were generated by Illumina sequencing and mapped with the BWA algorithm. Peaks were called using MACS and SICER. Only peaks > 120 were used in the comparative analysis.

Confocal imaging analysis

In vivo super-resolution confocal imaging of mitochondria was performed in young adult anesthetized (levamisole) nematodes carrying *ges-1p::gfp(mit)*, and adults fixed with 4% PFA in nematodes carrying *myo-3p::gfp(mit)*. Images were taken using the Zeiss Airyscan 2 LSM 900 equipped with a 63× oil objectives. Images were deconvoluted using Zen blue. Analysis of mitochondrial morphology was performed using Fiji 2.0.0 (open source).

CRISPR/Cas9 genome editing

A customized injection mix including sgRNAs targeting the coding sequence of *cest-2.2*, Cas9 protein, and a plasmid encoding *myo-2p:: GFP* was generated by NemaMetrix Inc. (Eugene OR, USA). Adult wild-type worms were microinjected with this custom mix, and the progeny was screened for GFP expression in the pharynx. GFP(+) worms were singled out and genotyped for the mutation until homozygosity was reached. The *cest-2.2(lf)* strain was then outcrossed twice before use in this study.

DNA constructs

The *cest-2.2p::cest-2.2::cest-2.2 3′UTR* plasmid was generated by ATG:biosynthetics GmbH (Merzhausen, Germany). The *unc-119* rescue cassette was cloned into the plasmid by digesting it with ApaI and SacII restriction enzymes followed by ligation, in order to make the plasmid compatible with biolistic transformation. A Gateway-compatible plasmid with the annotated sequence of the *cest-2.2* promoter was obtained from Dharmacon, Inc (Colorado, USA). The *cest-2.2* promoter was then cloned into a Gateway-compatible plasmid containing a *gfp:let-858 3′UTR* cassette with the 2-fragment Gateway method as per the manufacturer's instructions (Thermo Fisher Scientific, USA).

Egg-laying assay

Synchronized wt, *gas-1(fc21)* and *gas-1(fc21); cest-2.2 O/E* nematodes were placed on individual NGM plates seeded with OP50 at 3 days of age (L4 stage). Animals were transferred every day, and the eggs laid in each 24 h period were counted until the animal exited the egg-laying stage.

Fatty acid analysis

Synchronized 5-day-old nematodes were sorted with a COPAS Biosorter (~1,000 animals per samples), flash-frozen in liquid N_2, and stored at −80°C. For total lipid analysis, samples were extracted overnight in 5 ml chloroform:methanol (1:1, v:v). An aliquot of 500 μl of each sample was transferred in precleaned glass vials, the solvent was evaporated, and the samples were transesterified for 2 h at 80°C adding 2 ml of 1 N methanolic:HCl. Each sample was spiked with dotriacontane as an internal standard. The transesterification reaction was stopped by adding 2 ml of a saturated NaCl solution, and lipid monomers were extracted three times with hexane. Samples were derivatized by adding 20 μl N,O-bis (trimethylsilyl)-trifluoroacetamide (BSTFA; Machery-Nagel, Düren, Germany) and 20 μl pyridine (Sigma Aldrich, Deisenhofen, Germany) for 45 min at 70°C. For free fatty acid analysis, the respective TLC bands were scratched out, extracted in 5 ml chloroform, and analyzed as described above. For quantification 1 μl of each sample was analyzed by on column injection and gas chromatography equipped with flame ionization detection (GC-FID; CG-Hewlett-Packard 5890 series H, Hewlett-Packard, Palo Alto, CA, USA). For substance identification, 1 μl of each sample was analyzed by GC-MS (mass spectrometry, quadrupole mass selective detector HP 5971, Hewlett-Packard, Palo Alto, CA, USA).

Lifespan assays

All lifespan assays were performed at 20°C and without 5′-fluorodeoxyuridine (FUdR) supplementation. Gravid nematodes were treated with hypochlorite solution and eggs were placed on NGM plates seeded with *E. coli* OP50. For RNAi experiments, eggs were placed on NGM plates supplemented with ampicillin and seeded with *E. coli* HT115 bacteria carrying either an empty vector (pL4440) or plasmids expressing dsRNA against target genes (Ahringer library, Source Bioscience LifeSciences). Expression of dsRNA was induced by 1 mM isopropyl-β-d-1-thiogalactopyranoside. Adults were transferred every other day until egg laying was complete. Subsequently, nematodes were transferred twice per week and scored every other day by gentle prodding, and those that did not respond were scored as dead. Nematodes, which died of internal

egg hatching, protruded vulvas, or drying on the edge of the plates were censored.

Lipid staining

LipidTOX staining

Adult nematodes were collected in M9 buffer, washed, and fixed in 4% PFA for 15 min. PFA was removed, and worm pellets were permeabilized with three freeze/thaw cycles in liquid nitrogen. Worm pellets were washed three times in M9 then stained with 1:200 HCS LipidTOX Green Neutral Lipid Stain solution (Thermofisher) in M9 for 1.5 h at room temperature. Worms were washed three times with M9 and mounted onto glass slides in 100% glycerol. Images were taken using the Zeiss Airyscan 2 LSM 900 equipped with a 20× air objective and analyzed with Fiji 2.0.0 (open source).

ORO lipid staining

Adult nematodes were collected in M9 buffer, washed, and fixed in 1% PFA for 30 min. Fixed nematodes were then washed twice with M9 and incubated in 60% isopropanol for 15 min. Freshly prepared Oil Red O (ORO) stock solution (5mg/ml, in isopropanol) was diluted to 60% and used to stain the fixed nematodes overnight at RT. Samples were then washed three times in M9 and mounted onto glass slides in 100% glycerol. Brightfield images were acquired with an Axio Scan.Z1 slide scanner equipped with a 20× air objective (Zeiss). Images were analyzed with Fiji 2.0.0 (open source).

Locomotor activity

Nematodes were synchronized by NaClO/NaOH treatment and transferred every other day until they were 10 days old. At adulthood stage, 35 nematodes were manually transferred to a 96 well flat-bottom plate containing 100 μl of S medium and 6 mg/ml of filtered OP50, with a minimum of three wells analyzed per condition. The plate was placed into a WMicrotracker (Phylumtech S.A., Argentina) and the locomotory activity was recorded twice over 1 h.

Microparticle bombardment

Freshly starved *unc-119(ed3)* mutant nematodes were washed in M9 and placed on an unseeded NGM plate. Approximately 15 μg of plasmid DNA was added to 50 μl of 60 mg/ml gold particles, 20 μl of 0.1 M spermidine and 50 μl of 2.5 M CaCl$_2$. The suspension was pelleted, washed twice, and then resuspended in 170 μl of 100% ethanol. DNA-gold complexes were then spotted on microparticle carrier disks, and nematodes were bombarded with a Biolistic PDS/1000-He System (BIO-RAD). Bombarded animals were recovered in M9 and spotted on NGM plates with OP50. F1 animals were then screened and selected based on normal movement, and F2 animals were screened for homozygosity.

Next-generation sequencing (NGS)

We manually dissected 20 intestines from wt N2, *gas-1(fc21)* and *gas-1(fc21); cest-2.2* O/E animals (5 replicates each), which were then placed in 1 ml of Qiazol and snap-frozen in liquid nitrogen.

Total RNA was extracted using the miRNeasy Micro kit (Qiagen) according to manufacturer's protocol. RNA was quantified and RNA integrity was determined using the HS RNA assay on a Tapestation 4200 system (Agilent). Smart-seq2 was used for the generation of non-strand-specific, full transcript sequencing libraries using standard reagents and procedures as previously described (Picelli *et al*, 2014). Briefly, 1 ng of total RNA was transferred to buffer containing 0.2% TritonX-100, protein-based RNase inhibitor, dNTPs, and oligo-dT oligonucleotides to prime the subsequent RT reaction on polyadenylated mRNA sequences. The SMART RT reaction was performed at 42°C for 90 min using commercial SuperScript II (Invitrogen) and a TSO. A preamplification PCR of 14 cycles was performed to generate double-stranded DNA from the cDNA template. At least 200 pg of amplified cDNA were used for tagmentation reaction and subsequent PCR amplification using the Nextera XT kit (Illumina) to construct sequencing libraries. Libraries were quantified using the Qubit hs dsDNA assay, and library fragment size distribution was determined using the D1000 assay on a Tapestation 4200 system (Agilent). Samples were pooled and clustered at 1.4 pM on a NextSeq500 system (Illumina) to generate ~10 M single end reads per sample using High Output v2.5 chemistry. Sequencing data were demultiplexed using bcl2fastq2 v2.20 and pseudo aligned to *Caenorhabditis elegans*, WBcel235.98 transcriptome using kallisto v.0.44.0. Data analysis was performed using Shiny-Seq.

Oxygen consumption

Synchronized adult nematodes were placed on NGM plate seeded with heat-killed OP50 for 2 h. We manually transferred 50 nematodes per well to a Seahorse XF24 cell culture microplate in 525 μl of M9 buffer. Measurements were performed by using a Seahorse XF24 Analyzer (Agilent Technologies, USA). Nematodes were monitored for basal oxygen consumption and maximal respiration following an injection of 25 μM FCCP. To control for nonmitochondrial oxygen consumption, 20 mM sodium azide was finally injected.

Pharyngeal pumping

Pharyngeal pumping assay was performed using 5-day-old nematodes, which were placed on an NGM plate seeded with OP50 and left to acclimatize for at least 1 h. Pharyngeal pumps of individual animals were counted in a 60-s interval.

RNA extraction and quantitative real-time PCR

RNA was extracted from nematodes stored at −80°C with a QIAGEN RNeasy Kit as per the manufacturer's instructions. RNA was then retrotranscribed with qScript (Quantabio), and qRT-PCR was performed with SYBERgreen master mix (Applied Biosystems, USA) on an Applied Biosystems qRT-PCR Thermocycler. The following primers were used in this study:

acox-1.1 F: 5′-CTTCCAGCAAAGACCCTCGT-3′
acox-1.1 R: 5′-TCAGTTTGGGCGTAGGTTCC-3′
acs-2 F: 5′-CTATGTTCACACAATGCTTGAGG-3′
acs-2 R: 5′-TGGGATTTGATGTGTCCCAAC-3′
cest-2.2 F: 5′-TGTCAACTGGAACAATTGAAGGG-3′

cest-2.2 R: 5′-AACTCCGTCCCAGGGTTTTG-3′
ech-1.1 F: 5′-GCTGAGGCTAAGGCATTTGG-3′
ech-1.1 R: 5′-GACCGGAAGTCCTTTTCCGT-3′
fat-5 F: 5′-GCTCTACACATTGGAGCCCT-3′
fat-5 R: 5′-GTGTGCAGGAGGAATACCCA-3′
gst-4 F: 5′-GATACTTGGCAAGAAAATTTGGAC-3′
gst-4 F: 5′-TTGATCTACAATTGAATCAGCGTAA-3′
let-721 F: 5′-TGGGATGGCCATTGAATGTTG-3′
let-721 F: 5′-GCAACAACGAAACCAACGGA-3′
nhr-49 F: 5′-ACAAGTTGGAATGAAACGAGAAG-3′
nhr-49 R: 5′-TTGAATGGAGTCCCGTTGA-3′
nhr-80 F: 5′-ATCACCGACGAGATCATGCC-3′
nhr-80 R: 5′-TCGAAACCCCCTTGAAAGCA-3′
mdh-2 F: 5′-CTTCCAGCAAAGACCCTCGT-3′
mdh-2 R: 5′-AGAAGAGCGACCTTTGGAGC-3′
pck-1 F: 5′-ATTGGAAGAGACGAGGGATG-3′
pck-1 R: 5′-GGCGAGGTTGGTCTTTCC-3′
sod-3 F: 5′-CCAACCAGCGCTGAAATTCAATG-3′
sod-3 R: 5′-GGAACCGAAGTCGCGCTTAATAG-3′
vit-1 F: 5′-TCAAGGCTGACAAGAAGATCCAA-3′
vit-1 R: 5′-GCCTCGAGTGGAACGATGTC-3′
vit-2 F: 5′-CAAGGCTGACAAGAAGATCCA-3′
vit-2 R: 5′-GGGAGAATGTCCTCGTTTTCCA-3′
vit-3, 4, 5 F: 5′-GGCCGAGAAGAAGGTTCAACT-3′
vit-3, 4, 5 R: 5′-AGCTCAGCAGCTCTCAATGG-3′
vit-6 F: 5′-ACGATGAGCCAACTGAGCAA-3′
vit-6 R: 5′-GGCAGTAGACGGAGGTCTTTT-3′
actin F: 5′-TGTGATGCCAGATCTTCTCCAT-3′
actin R: 5′-GAGCACGGTATCGTCACCA-3′

Statistics

Statistical analyses listed in the Figure legends were performed with GraphPad Prism Software (San Diego, USA). All n numbers are reported and described in the Figure Legends.

SureQuant-based targeted mass spectrometry

Sample preparation

Adult wt and late L4 stage gas-1 (fc21) mutant and BAN329 gas-1 (fc21); cest-2.2 O/E nematodes were collected, washed twice with water, and stored at −80°C. Nematodes were washed twice with water, and the pellets were kept at −80°C. Samples were lysed in 200 µl Lysis buffer (50 mM HEPES (pH 7.4), 150 mM NaCl, 1 mM EDTA, 1.5% SDS, 1 mM DTT; supplemented with: 1× protease and phosphatase inhibitor cocktail). Lysis was aided by repeated cycles of sonication in a water bath (6 cycles of 1-min sonication (35 kHz) intermitted by 2-min incubation on ice). Approximately, 20 µg of C. elegans protein lysates were reduced and alkylated prior to processing by a modified filter-aided sample preparation (FASP) protocol as previously described (Scifo et al, 2015). Samples were digested overnight with trypsin (1:20; in 50 mM ammonium bicarbonate) directly on the filters, at 30°C, and precipitated using an equal volume of 2 M KCl for depletion of residual detergents. Tryptic peptides were then cleaned, desalted on C18 stage tips, and resuspended in 20 µl 1% FA for LC-MS analysis. MS runs were performed with 3 biological and 2 technical replicates.

Characterization of Stable isotope Labeled (SIL) Peptides

Synthetic PEPotec isotope-labeled c-terminal lysine (K) or arginine (R) crude peptides were purchased (Thermo Scientific), and an equimolar amount of each heavy peptide was mixed together at a final concentration of 1 pmol/µl in 0.1% FA to generate a pool of CEST-2.2 SIL peptides for subsequent nanoLC-MS/MS analysis to determine their intensities.

Liquid chromatography and Survey MS analyses

Endogenous and SIL peptides were mixed and injected with a flow rate of 300 nl/min, at starting conditions of 95% eluent A (0.1% FA in water) and 5% eluent B (0.1% FA in 80% ACN) for analysis on a Dionex Ultimate 3000 RSLC nanosystem coupled to an Orbitrap Exploris 480 MS. They were loaded onto a trap column cartridge (Acclaim PepMap C18 100 Å, 5 mm × 300 µm i.d., #160454, Thermo Scientific) and separated by reverse-phase chromatography on an Acclaim PepMap 100 C18 75 µm × 25 cm (both columns from Thermo Scientific) using a 35-min linear increasing gradient from 5 to 25% of eluent B followed by a 5-min linear increase to 50% eluent B. The mass spectrometer was operated in data-dependent and positive ion mode with a spray voltage of 1.9 kV, no sheath or auxiliary gas flow, heated capillary temperature of 300°C, MS1 spectra recorded at a resolution of 120K, mass scan range of 300–1,500, automatic gain control (AGC) target value of 300% $(3 × 10^6)$ ions, maximum injection time (maxIT) of 50 ms, and a default charge state of 2. For every scan, the top 40 most intense ions on the inclusion list (if above a 1e5 intensity threshold) were isolated within a width of 1.0 m/z and fragmented with a normalized collision energy (NCE) of 28% by higher energy collisional dissociation (HCD), scan range of 100–1,700 m/z, maximum IT of 10 ms, AGC target value of 1,000%, and resolution of 7,500.

SureQuant-based quantitation of selected CEST-2.2 tryptic peptides

SureQuant analysis was performed as previously described (Stopfer et al, 2021). Briefly, data acquisition was performed using a modified SureQuant template with 3 branches for the +2 (R, K), +3 (K) charge states of SIL lysine and arginine residues. Peak area ratios of endogenous light peptides and corresponding heavy IS peptides for the 6 selected product ions were exported from Skyline software v21.1.0.278 (MacLean et al 2010) and peptides filtered according to the following criteria: First, only IS peptides with an AUC > 0 for $n ≥ 5$ product ions were considered. Second, peak area values of the 3 highest intensity product ions from both the light/heavy peptides were summed, and their light/heavy ratios were used to quantify peptide signals across samples. Quantitation was based on 3 selected product ions to balance specificity with the ability to retain lowly abundant targets.

Thin layer chromatography

Animals at 5 days of age were sorted with a COPAS BioSorter, collected (1,000 animals per sample), flash-frozen, and stored at −80°C. Lipids were extracted by homogenizing pellets in 5 ml ExMi (chloroform–methanol–water 10:5:1 by volume) and then incubated at 48°C for 48 h. Denaturated proteins were then filtered from extract with cotton, and lipids were dried under an N_2 stream. Dried lipids were resuspended in ExMi and spotted on a silica gel plate

(Merck). Half of the plate was developed twice with chloroform–methanol–water (60:30:5 by volume), and then, the full plate was developed in hexane–diethyl ether–acetic acid (80:20:1.5 by volume). Lipids were visualized by charcoaling or alternatively by iodine vapors.

Treatments with oxaloacetate, NMN, ascorbate/vitamin C, and ascarosides

Standard NGM was prepared, supplemented with either 2 mM oxaloacetate or 1 mM nicotinamide mononucleotide (NMN) in aqueous solution, and the pH was adjusted with NaOH before pouring. Plates were seeded with OP50, and *gas-1(fc21)* mutants were grown on supplemented plates from hatching. Alternatively, plates were seeded with heat-killed OP50, and 4-day-old *gas-1(fc21)* mutants were placed on these plates for 24 h before collection. L-ascorbate/vitamin C was dissolved in MilliQ water and then filtered to obtain a sterile 10 mg/ml stock solution. Stock solution was added into the freshly prepared NGM to achieve a final concentration of 1 mg/ml. After pouring, plates were kept at 4°C until their use. Ascaroside ascr#8 and ascr#81 were synthesized and resuspended in 100% ethanol, then diluted to 50 μM solutions in dsH$_2$O for a final ethanol concentration of 1.7%. Both ascr#8 and ascr#81 (200 μl) or 1.7% ethanol (as control) were spread on the surface of 55 mm NGM plates and allowed to dry overnight (final concentration: 1 μM). The following day the plates were seeded with OP50, dried overnight and, *gas-1(fc21)* eggs were added.

Western blot analysis

Adult nematodes were washed three times with sterile water and the frozen at −80°C until protein extraction. Pellets were sonicated in ice-cold RIPA buffer (Sigma) with protease and phosphatase inhibitors. Lysates were cleared by centrifugation, total protein was determined by Bradford Assay (Sigma) and boiled in Laemmli buffer for 5 min. Approximately 20–40 μg of total protein was resolved on 10–15% polyacrylamide gels and subsequently transferred to nitrocellulose membranes using semi-dry transfer Trans-Blot Turbo™ (Bio-Rad). Following antibody incubation, membranes were developed in ECL and imaged using Chemidoc imaging system (Bio-Rad).

Data availability

The ChIP-Seq and the RNA-Seq in the gut have been deposited to NCBI GEO database under the common accession number GSE168502: https://www-ncbi-nlm-nih-gov.ezproxy.u-pec.fr/geo/browse/?view = samples&series = 168501

The RNA-Seq in *nuo-6(qm200)* versus wt and *nuo-6(qm200); his-72(tm2066); his-71(ok2289)* versus *nuo-6(qm200)* has been published in Piazzesi *et al* (2016). The RNA-Seq of g*as-1(fc21)* versus wt has been published in Gioran *et al* (2019).

Expanded View for this article is available online.

Author contributions

Antonia Piazzesi: Conceptualization; Supervision; Validation; Investigation; Writing—original draft. **Yiru Wang:** Validation; Investigation. **Joshua Jackson:** Investigation. **Lena Wischhof:** Investigation. **Viktoria Zeisler-Diehl:** Investigation. **Enzo Scifo:** Investigation. **Ina Oganezova:** Investigation. **Thorben Hoffmann:** Investigation. **Pablo Gomez Martin:** Investigation. **Fabio Bertan:** Investigation. **Chester J J Wrobel:** Methodology. **Frank C Schroeder:** Methodology. **Dan Ehninger:** Investigation. **Kristian Händler:** Investigation. **Joachim L Schultze:** Investigation. **Lukas Schreiber:** Investigation. **Gerhild van Echten-Deckert:** Investigation; TLC. **Pierluigi Nicotera:** Funding acquisition. **Daniele Bano:** Conceptualization; Supervision; Funding acquisition; Visualization; Writing—original draft; Project administration; Writing—review & editing.

Disclosure and competing interests statement

The authors declare that they have no conflict of interest.

References

Arantes-Oliveira N, Apfeld J, Dillin A, Kenyon C (2002) Regulation of life-span by germ-line stem cells in *Caenorhabditis elegans*. *Science* 295: 502 – 505

Askjaer P, Ercan S, Meister P (2014) Modern techniques for the analysis of chromatin and nuclear organization in *C. elegans*. *WormBook* 1 – 35

Ast T, Meisel JD, Patra S, Wang H, Grange RMH, Kim SH, Calvo SE, Orefice LL, Nagashima F, Ichinose F *et al* (2019) Hypoxia rescues frataxin loss by restoring iron sulfur cluster biogenesis. *Cell* 177: 1507 – 1521.e16

Bano D, Piazzesi A, Salomoni P, Nicotera P (2017) The histone variant H3.3 claims its place in the crowded scene of epigenetics. *Aging* 9: 602 – 614

Bano D, Prehn JHM (2018) Apoptosis-inducing factor (AIF) in physiology and disease: the tale of a repented natural Born killer. *EBioMedicine* 30: 29 – 37

Benedetti C, Haynes CM, Yang Y, Harding HP, Ron D (2006) Ubiquitin-like protein 5 positively regulates chaperone gene expression in the mitochondrial unfolded protein response. *Genetics* 174: 229 – 239

Bertan F, Wischhof L, Scifo E, Guranda M, Jackson J, Marsal-Cots A, Piazzesi A, Stork M, Peitz M, Prehn JHM *et al* (2021) Comparative analysis of CI- and CIV-containing respiratory supercomplexes at single-cell resolution. *Cell Rep Methods* 1: 100002 . https://doi.org/10.1016/j.crmeth.2021.100002

Brand MD, Nicholls DG (2011) Assessing mitochondrial dysfunction in cells. *Biochem J* 435: 297 – 312

Brock TJ, Browse J, Watts JL (2006) Genetic regulation of unsaturated fatty acid composition in *C. elegans*. *PLoS Genet* 2: e108

Brock TJ, Browse J, Watts JL (2007) Fatty acid desaturation and the regulation of adiposity in *Caenorhabditis elegans*. *Genetics* 176: 865–875

Calvo E, Cogliati S, Hernansanz-Agustin P, Loureiro-Lopez M, Guaras A, Casuso RA, Garcia-Marques F, Acin-Perez R, Marti-Mateos Y, Silla-Castro JC *et al* (2020) Functional role of respiratory supercomplexes in mice: SCAF1 relevance and segmentation of the Qpool. *Sci Adv* 6: eaba7509

Cantó C, Houtkooper R, Pirinen E, Youn D, Oosterveer M, Cen Y, Fernandez-Marcos P, Yamamoto H, Andreux PA, Cettour-Rose P *et al* (2012) The NAD(+) precursor nicotinamide riboside enhances oxidative metabolism and protects against high-fat diet-induced obesity. *Cell Metab* 15: 838–847

Cerutti R, Pirinen E, Lamperti C, Marchet S, Sauve A, Li W, Leoni V, Schon E, Dantzer F, Auwerx J *et al* (2014) NAD(+)-dependent activation of Sirt1 corrects the phenotype in a mouse model of mitochondrial disease. *Cell Metab* 19: 1042–1049

Chen AL, Lum KM, Lara-Gonzalez P, Ogasawara D, Cognetta AB, To A, Parsons WH, Simon GM, Desai A, Petrascheck M *et al* (2019) Pharmacological convergence reveals a lipid pathway that regulates *C. elegans* lifespan. *Nat Chem Biol* 15: 453–462

Chen WW, Lemieux GA, Camp Jr CH, Chang TC, Ashrafi K, Cicerone MT (2020) Spectroscopic coherent Raman imaging of *Caenorhabditis elegans* reveals lipid particle diversity. *Nat Chem Biol* 16: 1087–1095

Cracan V, Titov DV, Shen H, Grabarek Z, Mootha VK (2017) A genetically encoded tool for manipulation of NADP(+)/NADPH in living cells. *Nat Chem Biol* 13: 1088–1095

Dillin A, Hsu AL, Arantes-Oliveira N, Lehrer-Graiwer J, Hsin H, Fraser AG, Kamath RS, Ahringer J, Kenyon C (2002) Rates of behavior and aging specified by mitochondrial function during development. *Science* 298: 2398–2401

Durieux J, Wolff S, Dillin A (2011) The cell-non-autonomous nature of electron transport chain-mediated longevity. *Cell* 144: 79–91

Eaton S (2002) Control of mitochondrial beta-oxidation flux. *Prog Lipid Res* 41: 197–239

Felkai S, Ewbank JJ, Lemieux J, Labbe JC, Brown GG, Hekimi S (1999) CLK-1 controls respiration, behavior and aging in the nematode *Caenorhabditis elegans*. *EMBO J* 18: 1783–1792

Feng J, Bussière F, Hekimi S (2001) Mitochondrial electron transport is a key determinant of life span in *Caenorhabditis elegans*. *Dev Cell* 1: 633–644

Frazier AE, Thorburn DR, Compton AG (2019) Mitochondrial energy generation disorders: genes, mechanisms, and clues to pathology. *J Biol Chem* 294: 5386–5395

Van Gilst MR, Hadjivassiliou H, Jolly A, Yamamoto KR (2005) Nuclear hormone receptor NHR-49 controls fat consumption and fatty acid composition in *C. elegans*. *PLoS Biol* 3: e53

Gioran A, Piazzesi A, Bertan F, Schroer J, Wischhof L, Nicotera P, Bano D (2019) Multi-omics identify xanthine as a pro-survival metabolite for nematodes with mitochondrial dysfunction. *EMBO J* 38: e99558

Gorman GS, Chinnery PF, DiMauro S, Hirano M, Koga Y, McFarland R, Suomalainen A, Thorburn DR, Zeviani M, Turnbull DM (2016) Mitochondrial diseases. *Nat Rev Dis Primers* 2: 16080

Grange RMH, Sharma R, Shah H, Reinstadler B, Goldberger O, Cooper MK, Nakagawa A, Miyazaki Y, Hindle AG, Batten AJ *et al* (2021) Hypoxia ameliorates brain hyperoxia and NAD(+) deficiency in a murine model of Leigh syndrome. *Mol Genet Metab* 133: 83–93

Greer EL, Maures TJ, Ucar D, Hauswirth AG, Mancini E, Lim JP, Benayoun BA, Shi Y, Brunet A (2011) Transgenerational epigenetic inheritance of longevity in *Caenorhabditis elegans*. *Nature* 479: 365–371

Han S, Schroeder EA, Silva-Garcia CG, Hebestreit K, Mair WB, Brunet A (2017) Mono-unsaturated fatty acids link H3K4me3 modifiers to *C. elegans* lifespan. *Nature* 544: 185–190

Harvald EB, Sprenger RR, Dall KB, Ejsing CS, Nielsen R, Mandrup S, Murillo AB, Larance M, Gartner A, Lamond AI *et al* (2017) Multi-omics analyses of starvation responses reveal a central role for lipoprotein metabolism in acute starvation survival in *C. elegans*. *Cell Syst* 5: 38–52.e4

Haynes CM, Yang Y, Blais SP, Neubert TA, Ron D (2010) The matrix peptide exporter HAF-1 signals a mitochondrial UPR by activating the transcription factor ZC376.7 in *C. elegans*. *Mol Cell* 37: 529–540

Imanikia S, Sheng M, Castro C, Griffin JL, Taylor RC (2019) XBP-1 remodels lipid metabolism to extend longevity. *Cell Rep* 28: 581–589.e4

Ising C, Koehler S, Brähler S, Merkwirth C, Höhne M, Baris OR, Hagmann H, Kann M, Fabretti F, Dafinger C *et al* (2015) Inhibition of insulin/IGF-1 receptor signaling protects from mitochondria-mediated kidney failure. *EMBO Mol Med* 7: 275–287

Jain IH, Calvo SE, Markhard AL, Skinner OS, To TL, Ast T, Mootha VK (2020) Genetic screen for cell fitness in high or low oxygen highlights mitochondrial and lipid metabolism. *Cell* 181: 716–727.e11

Jain IH, Zazzeron L, Goli R, Alexa K, Schatzman-Bone S, Dhillon H, Goldberger O, Peng J, Shalem O, Sanjana NE *et al* (2016) Hypoxia as a therapy for mitochondrial disease. *Science* 352: 54–61

Jain IH, Zazzeron L, Goldberger O, Marutani E, Wojtkiewicz GR, Ast T, Wang H, Schleifer G, Stepanova A, Brepoels K *et al* (2019) Leigh syndrome mouse model can be rescued by interventions that normalize brain hyperoxia, but not HIF activation. *Cell Metab* 30: 824–832.e3

Johnson AA, Stolzing A (2019) The role of lipid metabolism in aging, lifespan regulation, and age-related disease. *Aging Cell* 18. https://doi.org/10.1111/acel.13048

Johnson SC, Yanos ME, Kayser E-B, Quintana A, Sangesland M, Castanza A, Uhde L, Hui J, Wall VZ, Gagnidze A *et al* (2013) mTOR inhibition alleviates mitochondrial disease in a mouse model of Leigh syndrome. *Science* 342: 1524–1528

Karamanlidis G, Lee CF, Garcia-Menendez L, Kolwicz Jr SC, Suthammarak W, Gong G, Sedensky MM, Morgan PG, Wang W, Tian R (2013) Mitochondrial complex I deficiency increases protein acetylation and accelerates heart failure. *Cell Metab* 18: 239–250

Khan NA, Nikkanen J, Yatsuga S, Jackson C, Wang L, Pradhan S, Kivela R, Pessia A, Velagapudi V, Suomalainen A (2017) mTORC1 regulates mitochondrial integrated stress response and mitochondrial myopathy progression. *Cell Metab* 26: 419–428.e5

Kimble J, Sharrock WJ (1983) Tissue-specific synthesis of yolk proteins in *Caenorhabditis elegans*. *Dev Biol* 96: 189–196

Klapper M, Ehmke M, Palgunow D, Böhme M, Matthäus C, Bergner G, Dietzek B, Popp J, Döring F (2011) Fluorescence-based fixative and vital staining of lipid droplets in *Caenorhabditis elegans* reveal fat stores using microscopy and flow cytometry approaches. *J Lipid Res* 52: 1281–1293

Koopman WJH, Distelmaier F, Smeitink JAM, Willems PHGM (2012) OXPHOS mutations and neurodegeneration. *EMBO J* 32: 9–29

Lake NJ, Compton AG, Rahman S, Thorburn DR (2016) Leigh syndrome: one disorder, more than 75 monogenic causes. *Ann Neurol* 79: 190–203

Lakowski B, Hekimi S (1996) Determination of life-span in *Caenorhabditis elegans* by four clock genes. *Science* 272: 1010–1013

Lardenoije R, Iatrou A, Kenis G, Kompotis K, Steinbusch HWM, Mastroeni D, Coleman P, Lemere CA, Hof PR, van den Hove DLA *et al* (2015) The epigenetics of aging and neurodegeneration. *Prog Neurogibol* 131: 21–64

Le HH, Wrobel CJ, Cohen SM, Yu J, Park H, Helf MJ, Curtis BJ, Kruempel JC, Rodrigues PR, Hu PJ *et al* (2020) Modular metabolite assembly in *C. elegans* depends on carboxylesterases and formation of lysosome-related organelles. *Elife* 9: e61886

Lee SS, Lee RY, Fraser AG, Kamath RS, Ahringer J, Ruvkun G (2003) A systematic RNAi screen identifies a critical role for mitochondria in *C. elegans* longevity. *Nat Genet* 33: 40−48

Lin Y-F, Haynes CM (2016) Metabolism and the UPR(mt). *Mol Cell* 61: 677−682

Liu S, Fu S, Wang G, Cao YU, Li L, Li X, Yang J, Li N, Shan Y, Cao Y *et al* (2021) Glycerol-3-phosphate biosynthesis regenerates cytosolic NAD(+) to alleviate mitochondrial disease. *Cell Metab* 33: 1974−1987.e9

Ludewig AH, Schroeder FC (2013) Ascaroside signaling in *C. elegans*. *WormBook* 1−22

MacLean B, Tomazela DM, Shulman N, Chambers M, Finney GL, Frewen B, Kern R, Tabb DL, Liebler DC, MacCoss MJ (2010) Skyline: an open source document editor for creating and analyzing targeted proteomics experiments. *Bioinformatics* 26: 966−968

Martinez-Reyes I, Chandel NS (2020) Mitochondrial TCA cycle metabolites control physiology and disease. *Nat Commun* 11: 102

McKay RM, McKay JP, Avery L, Graff JM (2003) C elegans: a model for exploring the genetics of fat storage. *Dev Cell* 4: 131−142

Merkwirth C, Jovaisaite V, Durieux J, Matilainen O, Jordan S, Quiros P, Steffen K, Williams E, Mouchiroud L, Tronnes S *et al* (2016) Two conserved histone demethylases regulate mitochondrial stress-induced longevity. *Cell* 165: 1209−1223

Mottis A, Herzig S, Auwerx J (2019) Mitocellular communication: shaping health and disease. *Science* 366: 827−832

Mouchiroud L, Houtkooper R, Moullan N, Katsyuba E, Ryu D, Cantó C, Mottis A, Jo Y-S, Viswanathan M, Schoonjans K *et al* (2013) The NAD(+)/Sirtuin pathway modulates longevity through activation of mitochondrial UPR and FOXO signaling. *Cell* 154: 430−441

Nargund AM, Pellegrino MW, Fiorese CJ, Baker BM, Haynes CM (2012) Mitochondrial import efficiency of ATFS-1 regulates mitochondrial UPR activation. *Science* 337: 587−590

Ooi SL, Priess JR, Henikoff S (2006) Histone H3.3 variant dynamics in the germline of *Caenorhabditis elegans*. *PLoS Genet* 2: e97. https://doi.org/10.1371/journal.pgen.0020097

O'Rourke EJ, Ruvkun G (2013) MXL-3 and HLH-30 transcriptionally link lipolysis and autophagy to nutrient availability. *Nat Cell Biol* 15: 668−676

Peng M, Ostrovsky J, Kwon YJ, Polyak E, Licata J, Tsukikawa M, Marty E, Thomas J, Felix CA, Xiao R *et al* (2015) Inhibiting cytosolic translation and autophagy improves health in mitochondrial disease. *Hum Mol Genet* 24: 4829−4847

Perez MF, Lehner B (2019) Vitellogenins - yolk gene function and regulation in *Caenorhabditis elegans*. *Front Physiol* 10: 1067

Pfleger J, He M, Abdellatif M (2015) Mitochondrial complex II is a source of the reserve respiratory capacity that is regulated by metabolic sensors and promotes cell survival. *Cell Death Dis* 6: e1835

Piazzesi A, Papic D, Bertan F, Salomoni P, Nicotera P, Bano D (2016) Replication-independent histone variant H3.3 controls animal lifespan through the regulation of pro-longevity transcriptional programs. *Cell Rep* 17: 987−996

Picelli S, Faridani OR, Bjorklund AK, Winberg G, Sagasser S, Sandberg R (2014) Full-length RNA-seq from single cells using Smart-seq2. *Nat Protoc* 9: 171−181

Pirinen E, Cantó C, Jo Y, Morato L, Zhang H, Menzies K, Williams E, Mouchiroud L, Moullan N, Hagberg C *et al* (2014) Pharmacological Inhibition of poly(ADP-ribose) polymerases improves fitness and mitochondrial function in skeletal muscle. *Cell Metab* 19: 1034−1041

Quirós PM, Mottis A, Auwerx J (2016) Mitonuclear communication in homeostasis and stress. *Nat Rev Mol Cell Biol* 17: 213−226

Rahman MM, Rosu S, Joseph-Strauss D, Cohen-Fix O (2014) Down-regulation of tricarboxylic acid (TCA) cycle genes blocks progression through the first mitotic division in *Caenorhabditis elegans* embryos. *Proc Natl Acad Sci USA* 111: 2602−2607

Rea SL, Ventura N, Johnson TE (2007) Relationship between mitochondrial electron transport chain dysfunction, development, and life extension in *Caenorhabditis elegans*. *PLoS Biol* 5: e259

Riera CE, Merkwirth C, De Magalhaes Filho CD, Dillin A (2016) Signaling networks determining life span. *Annu Rev Biochem* 85: 35−64

Rossignol R, Faustin B, Rocher C, Malgat M, Mazat JP, Letellier T (2003) Mitochondrial threshold effects. *Biochem J* 370: 751−762

Russell OM, Gorman GS, Lightowlers RN, Turnbull DM (2020) Mitochondrial diseases: hope for the future. *Cell* 181: 168−188

Schmeisser S, Li S, Bouchard B, Ruiz M, Des Rosiers C, Roy R (2019) Muscle-specific lipid hydrolysis prolongs lifespan through global lipidomic remodeling. *Cell Rep* 29: 4540−4552.e8

Schon EA, Przedborski S (2011) Mitochondria: the next (neurode)generation. *Neuron* 70: 1033−1053

Scifo E, Szwajda A, Soliymani R, Pezzini F, Bianchi M, Dapkunas A, Dębski J, Uusi-Rauva K, Dadlez M, Gingras A-C *et al* (2015) Proteomic analysis of the palmitoyl protein thioesterase 1 interactome in SH-SY5Y human neuroblastoma cells. *J Proteomics* 123: 42−53

Seah NE, de Magalhaes Filho CD, Petrashen AP, Henderson HR, Laguer J, Gonzalez J, Dillin A, Hansen M, Lapierre LR (2016) Autophagy-mediated longevity is modulated by lipoprotein biogenesis. *Autophagy* 12: 261−272

Shpilka T, Haynes CM (2018) The mitochondrial UPR: mechanisms, physiological functions and implications in ageing. *Nat Rev Mol Cell Biol* 19: 109−120

Siegmund S, Yang H, Sharma R, Javors M, Skinner O, Mootha V, Hirano M, Schon EA (2017) Low-dose rapamycin extends lifespan in a mouse model of mtDNA depletion syndrome. *Hum Mol Genet* 26: 4588−4605

Sies H, Jones DP (2020) Reactive oxygen species (ROS) as pleiotropic physiological signalling agents. *Nat Rev Mol Cell Biol* 21: 363−383

Spinelli JB, Haigis MC (2018) The multifaceted contributions of mitochondria to cellular metabolism. *Nat Cell Biol* 20: 745−754

Stopfer LE, Flower CT, Gajadhar AS, Patel B, Gallien S, Lopez-Ferrer D, White FM (2021) High-density, targeted monitoring of tyrosine phosphorylation reveals activated signaling networks in human tumors. *Cancer Res* 81: 2495−2509

Tian Y, Garcia G, Bian Q, Steffen KK, Joe L, Wolff S, Meyer BJ, Dillin A (2016a) Mitochondrial stress induces chromatin reorganization to promote longevity and UPR(mt). *Cell* 165: 1197−1208

Tian Y, Merkwirth C, Dillin A (2016b) Mitochondrial UPR: a double-edged sword. *Trends Cell Biol* 26: 563−565

To TL, Cuadros AM, Shah H, Hung WHW, Li Y, Kim SH, Rubin DHF, Boe RH, Rath S, Eaton JK *et al* (2019) A compendium of genetic modifiers of mitochondrial dysfunction reveals intra-organelle buffering. *Cell* 179: 1222−1238 e1217

Troulinaki K, Bano D (2012) Mitochondrial deficiency: a double-edged sword for aging and neurodegeneration. *Front Genet* 3: 244

Troulinaki K, Büttner S, Marsal Cots A, Maida S, Meyer K, Bertan F, Gioran A, Piazzesi A, Fornarelli A, Nicotera P *et al* (2018) WAH-1/AIF regulates mitochondrial oxidative phosphorylation in the nematode *Caenorhabditis elegans*. *Cell Death Discov* 4: 2

Wallace DC (2018) Mitochondrial genetic medicine. *Nat Genet* 50: 1642−1649

Wang MC, O'Rourke EJ, Ruvkun G (2008) Fat metabolism links germline stem cells and longevity in *C. elegans*. *Science* 322: 957−960

Wang Y, Palmfeldt J, Gregersen N, Makhov AM, Conway JF, Wang M, McCalley SP, Basu S, Alharbi H, St. Croix C *et al* (2019) Mitochondrial fatty acid oxidation and the electron transport chain comprise a multifunctional mitochondrial protein complex. *J Biol Chem* 294: 12380−12391

Watts JL, Ristow M (2017) Lipid and carbohydrate metabolism in *Caenorhabditis elegans. Genetics* 207: 413−446

van der Windt GJ, Everts B, Chang CH, Curtis JD, Freitas TC, Amiel E, Pearce EJ, Pearce EL (2012) Mitochondrial respiratory capacity is a critical regulator of CD8+ T cell memory development. *Immunity* 36: 68−78

Wischhof L, Gioran A, Sonntag-Bensch D, Piazzesi A, Stork M, Nicotera P, Bano D (2018) A disease-associated Aifm1 variant induces severe myopathy in knockin mice. *Mol Metab* 13: 10−23

Yang W, Hekimi S (2010) A mitochondrial superoxide signal triggers increased longevity in *Caenorhabditis elegans. PLoS Biol* 8: e1000556

Zheng X, Boyer L, Jin M, Kim Y, Fan W, Bardy C, Berggren T, Evans RM, Gage FH, Hunter T (2016) Alleviation of neuronal energy deficiency by mTOR inhibition as a treatment for mitochondria-related neurodegeneration. *Elife* 5: e13378